



**University of  
Zurich** <sup>UZH</sup>

Department of Geography

# General Flowering in Malaysian Borneo shown in Spatial Variability of Phenocam Indices

GEO 610 Master's Thesis

**Author**

Joan Tracy Sturm  
12-709-051

**Supervised by**

Dr. Rogier De Jong

**Faculty representative**

Prof. Dr. Michael Schaepman

03.08.2018

Department of Geography, University of Zurich



## **Abstract**

General flowering is a unique aseasonal phenological event in the tropical dipterocarp forests of Southeast Asia. During this phenomenon, hundreds of different plant species from various taxonomic levels synchronise flowering and fruiting. The flowering events of each species last about two weeks and the combined event may extend to three months. Likely triggers include drought, temperature drops, high solar radiation in combination with seedling survival strategies and stored nutrients. The reproductive event has a great impact on the economy as well as forest management strategies. The study site is located in the Lambir Hills National Park, Malaysian Borneo. This region is one of the world's biodiversity hotspots and has a perhumid climate that is regularly confronted with extreme weather events.

Phenocam and satellite observations may reveal these important ecological events. In this study, data from the Phenological Eyes Network dating from 2013 to 2016 was analysed and compared to results from satellite data from Landsat 7, Landsat 8 and Sentinel-2A. Common vegetation indices, such as NDVI, saturate at high vegetation densities. The red chromatic coordinate (RCC) as the ratio of red light to green and blue light from the visible wavelength spectrum is less sensitive to this effect and was used to detect white and yellow flowers on the green canopy background. Furthermore, upscaling from the high spatial resolution of the phenocam image to the moderate spatial resolution representing a satellite pixel was tested. Finally, the theory of drought being the most likely trigger was tested using various drought definitions on the rainfall data of the global precipitation measurement mission.

The RCC analysis on the phenocam imagery revealed a correlation of the RCC variance between the differently sized sample patches and general flowering events recorded in the literature. The observational scale had a considerable influence on the strength and timing of the signal. However, no significant correlations were found for the satellite imagery. This indicates that spatial resolution and revisit time are crucial factors for successful detection of flowering events. Drought indices showed periods of low precipitation before the general flowering events but also further droughts without a subsequent flowering. Drought may thus be a trigger while not every drought event triggers flowering. The relation with other possible triggers and spatial relations of triggers and phenomenon were not included in this study.

RCC variance did indeed reveal a signal correlating with general flowering events but with a time lag of one to three months. The peak of the RCC variance signal rather shows the fruits of the canopy trees than the flowers. As the fruits depend on preceding flowering, however, the signal can be used as a proxy for general flowering. The signal for the biggest sample patches followed the same patterns as the signal at finer spatial resolution and, therefore, flowering detection should

be possible with satellite imagery. Practically, this does not work yet, as cloud contamination lowers the image density to a level where no distinct correlation between the signal from the satellite imagery and general flowering events can be found.

## Table of contents

Abstract .....	iii
List of figures .....	vii
List of tables .....	ix
List of abbreviations .....	x
1. Introduction .....	1
1.1. Research questions .....	2
2. General flowering .....	3
2.1. Relevance .....	4
2.2. Potential triggers .....	5
2.3. Observing flowering events .....	7
2.3.1. In-situ observations .....	7
2.3.2. Phenocam imagery .....	8
2.3.3. Satellite imagery .....	8
3. Study site .....	10
3.1. Site characteristics .....	10
3.2. Climate regime .....	11
4. Data & methods .....	13
4.1. In-situ data .....	13
4.2. Phenocam imagery .....	15
4.2.1. Phenological Eyes Network .....	16
4.2.2. Data preparation .....	17
4.3. Satellite data .....	18
4.3.1. Satellite imagery .....	19
4.3.2. Precipitation Measurement Missions .....	20
4.4. Flowering metrics .....	20
4.4.1. Red-edge indices .....	21
4.4.2. Visible-light indices .....	21
4.4.3. Observational scale .....	23
4.5. Quantification of dry periods .....	24
5. Results .....	25
5.1. Chromaticity coordinates from the phenocam imagery .....	25
5.1.1. RCC mean .....	27
5.1.2. RCC variance .....	27

5.2. Validation .....	27
5.3. Process scale of flowering .....	28
5.4. Satellite time series .....	29
5.5. Correlation of general flowering events and drought patterns .....	30
6. Discussion .....	32
6.1. General flowering shown by Red Chromatic Coordinate .....	32
6.2. Links to leaf flushing and masting .....	33
6.2.1. Leaf flushing .....	33
6.2.2. Masting .....	34
6.3. Importance of the observational scale .....	35
6.4. Defining possible triggers .....	36
6.5. Outlook: satellite remote sensing .....	36
7. Conclusion .....	38
8. Acknowledgments .....	39
9. References .....	40

## List of figures

- Fig. 1: The interaction between climate and weather extremes in tropical and subtropical regions and the impact on tree phenology and further impacts on dependent fauna and ecosystem functions. Natural variability in climate like El Niño-Southern Oscillation (ENSO), Pacific decadal oscillation (PDO), Indian Ocean Dipole (IOD), intertropical convergence zone (ITCZ) and Madden-Julian oscillation (MJO) are affected by natural and anthropogenic drivers. They can influence climate extremes through changes in the hydrological cycle, temperature regime and storm events. These in turn affect phenological events like flowering, budding and fruiting. Dependant nectar and fruit availability is vital for vertebrates. Further, ecosystem services like pollination, seed dispersal and forest regeneration depending on tree phenology might alter community composition and species' persistence. Schematic representation taken from Butt et al. (2015)..... 5
- Fig. 2: The location of Lambir Hills National Park (4°11'44"N, 114°02'26"E) in the province Sarawak in Malaysian Borneo..... 10
- Fig. 3: General flowering events (grey bars) and visualised data availability at Lambir Hills National Park. In-situ observations have been acquired biweekly, two daily phenocam imagery datasets from the Phenological Eye Network (PEN) are available, and numerous satellite imagery is available for free at varying spatial and temporal resolutions. MODIS on board of Terra and Aqua provides daily coverage at 250m/500m/1km. The Landsat satellites deliver global coverage every 16 days at 30m spatial resolution with a 15m panchromatic band for Landsat 7 and Landsat 8. The twin mission with the satellites Sentinel-2A and Sentinel-2B (launched in 2017) provides a combined global coverage within five days at 10m/20m/60m..... 13
- Fig. 4: Flowering ratio – The proportion of flowering individuals out of 207 observed canopy plants in total. Biweekly in-situ observations collected over the time span of 18 years at Lambir Hills National Park..... 14
- Fig. 5: Flowering periods of the canopy dominating *Dipterocarpaceae* family in Lambir Hills National Park during the general flowering of 1996. Data collected from the tree tower in Lambir Hills National Park by Roubik et al. (2005), figure taken from Sakai and Itioka (2016)..... 15
- Fig. 6: Selection representing the variation of the phenocam imagery from the Phenological Eyes Network: a) Sunny weather allows a perfect view on the canopy; b) Cloud shadows cover the canopy partially; c) The full camera's field of view lays in the shade; d) Overexposure; e) Image taken at dusk due to malfunctioning timer; f) Backlighting and

lens flares; g) Fog; h) Condensation on lens; i) Loose building material hanging in front of the camera; j) The camera fell and the field of view changed totally. Data source see Section 4.2.1..... 17

Fig. 7: Region of interest sample sizes computed with the simple linear iterative clustering algorithm: a) Reference image with superpixel boundaries for clusters representing approximately an individual tree crown; b) The means of a very fine scale subdivision of tree crowns – shaded parts of the canopy are divided from illuminated parts; c) The means of a fine scale subdivision; d) The means of subdivision of tree crowns into two or three parts; e) The means of superpixels representing an individual tree crown; f) The means of two tree crowns; g) Of three tree crowns; h) And of approximately five tree crowns.....23

Fig. 8: RGB chromatic coordinates (CC): a) Mean values of the CC sampled over the smallest observational scale from the eastern facing camera; b) The variance of the CC between the sampled patches facing East; c) Mean values sampled over the smallest observational scale from the western facing camera; d) The variance of the CC between the sampled patches facing West..... 25

Fig. 9: The statistical mean (continuous line; 0.3187) and the range where 95% of the values lay within, defined by two standard deviations (dashed lines) from the mean of the red chromatic coordinates (RCC; red dots) from the smallest sample size. The statistics have been calculated for the years 2013 (a), 2014 (b), and 2016 (c) as relatively continuous datasets from the eastern facing camera are available for these years..... 26

Fig. 10: The statistical mean (continuous line;  $1.9476 \cdot 10^{-4}$ ) and the range where 95% of the values lay within, defined by two standard deviations (dashed lines) from the variance of the red chromatic coordinates (RCC; red dots) from the smallest sample size. The statistics have been calculated for the years 2013 (a), 2014 (b), and 2016 (c) as relatively continuous datasets from the eastern facing camera are available for these years..... 26

Fig. 11: The variance of red chromatic coordinates from the eastern facing phenocam at Lambir Hills National Park for 2014. The signals are sorted according to an observational scale from the smallest sample size representing a part of a tree canopy (approximately 2\*2m) to several trees in one sample (approximately 25\*25m)..... 28

Fig. 12: Comparison of the RCC variance from the phenocam and satellite imagery. a) RCC variance of the eastern facing phenocam in Lambir Hills National Park (LHNP) over the biggest sample size (approximately 25\*25m); b) RCC variance derived over the whole LHNP area from cloud free Landsat 7 surface reflectance (SR) imagery, with a pixel

size of 30\*30m; c) RCC variance derived over the whole LHNP area from cloud free Landsat 8 SR imagery, with a pixel size of 30\*30m; d) RCC variance derived over the whole LHNP area from cloud free Sentinel-2A top of atmosphere imagery, with a pixel size of 10\*10m..... 30

Fig. 13: Precipitation values and droughts at Lambir Hills National Park for the years 2012 to 2016: a) daily precipitation values from the PMM; b) periods with total rainfall amount <100mm for 30 continuous days (Brunig, 1969; Harrison, 2001); c) periods with total rainfall amount <200mm for 3 continuous months (Azmy et al., 2016); d) periods with total rainfall amount <40mm for 30 continuous days (Sakai et al., 2006); e) periods with total rainfall amount <40mm for 14 continuous days (Kurten et al., 2017); f) periods with total rainfall amount <5mm for 14 continuous days (Ichie et al., 2004)..... 31

### List of tables

Tab. 1: Varying drought definitions applied in literature and general flowering research in Southeast Asia..... 24

Tab. 2: Different applied observational sample sizes from a region of interest representing a part of a tree canopy to several trees in one sample. And the highest red chromatic coordinate (RCC) variance between the samples in one image of the phenocam imagery facing East over the year 2014 as well as the date when the highest RCC variance value was measured..... 29

## **List of abbreviations**

ADFC	Automatic digital fish-eye camera
BCC	Blue chromatic coordinate
BRDF	Bidirectional reflectance distribution function
CC	Chromaticity Coordinates
CERES	Cloud and Earth Radiant Energy Sensor
ENSO	El Niño Southern Oscillation
ESA	European Space Agency
ETM+	Enhanced Thematic Mapper Plus
EVI	Enhanced vegetation index
GCC	Green chromatic coordinate
GEE	Google Earth Engine
GPM	Global Precipitation Measurement
GRVI	Green-red vegetation index
HSSR	HemiSpherical SpectroRadiometer
IOD	Indian Ocean Dipole
ITCZ	Intertropical convergence zone
JAXA	Japan Aerospace Exploration Agency
LHNP	Lambir Hills National Park
LIS	Lightning Imaging Sensor
MJO	Madden-Julian oscillation
MMU	Minimal mapping unit
MODIS	Moderate-imaging resolution spectroradiometer
MSI	Multispectral Imager
MSS	Multispectral Scanner System
NASA	National Aeronautics and Space Administration
NDVI	Normalized difference vegetation index
NIR	Near-infrared
OLI	Operational Land Imager
PDO	Pacific decadal oscillation
PEN	Phenological Eyes Network
PMM	Precipitation Measurement Missions
PR	Precipitation Radar
RCC	Red chromatic coordinate

RCP	Representative Concentration Pathway
ROI	Region of interest
RSL	Remote Sensing Laboratories
SLC	Scan line corrector
SP	Sun Photometer
TIRS	Thermal Infrared Sensor
TM	Thematic Mapper
TMI	TRMM Microwave Imager
TRMM	Tropical Rainfall Measuring Mission
URPP	University of Zurich Research Priority Program
UZH	University of Zurich
VIRS	Visible and InfraRed Scanner



## 1. Introduction

Incremental evolution, based on environmental conditions, equipped plants for their survival and led to their existence in a certain habitat (Fitchett et al., 2015). Southeast Asia's climate supports a year-round plant growth, which is favourable for the evergreen tropical rainforest in that region (Ichie et al., 2004). Recently, increased human population, logging, and intensified agriculture repressed the forests and divided them into smaller patches (Harrison, 2001). Furthermore, currently changing climate conditions may affect habitat suitability (Fitchett et al., 2015) and local species will likely respond by changing their abundance, range, and seasonal timing of life cycle events. Park and Miura (2011) also expect extreme events, such as El Niño, to become more frequent and significantly influence vegetation dynamics in tropical regions.

Tropical forests play a crucial component in regional and global biological mechanisms (Park & Miura, 2011). The interaction of biosphere and atmosphere is particularly important when it comes to carbon cycling and sequestration. Storing a fifth of the terrestrial carbon stock, tropical forests are a vital carbon sink (Nagai et al., 2016; Park & Miura, 2011; Yan et al., 2017). In addition to this, tropical forests account for about a third of the global net primary productivity and the ecosystem functions photosynthesis and evapotranspiration may alter global heat, water, and carbon-cycles (Nagai et al., 2016).

Phenology, the study of periodic biological life cycle stages (Lieth, 1974; Schwartz, 2003), offers insight into the impact of changing climate on ecosystems due to its interaction with the weather (Fitchett et al., 2015; Moore et al., 2016; Richardson et al., 2013). Phenology, as an essential biodiversity variable as proposed by Pereira et al. (2013), could be used to improve and develop climate models as well as in the monitoring of biodiversity change (Böttcher et al., 2016; Fitchett et al., 2015; Morisette et al., 2009; Pereira et al., 2013). Changes in phenology belong to species' first response to climate change, hence, the high descriptive potential of this value (Diez et al., 2012). Across the tropics, the main drivers of phenology shifts are changes in the occurrence and strength of precipitation and temperature extremes rather than changes in mean climate as common in the mid and high latitudes (Alberton et al., 2017; Butt et al., 2015; Fitchett et al., 2015). Examples for these changes are severe droughts, heat waves, floods and cyclones (Butt et al., 2015). These changes in weather extremes may influence the flowering – and thus reproduction – regime of the dipterocarp forest.

## **1.1. Research questions**

Detection of general flowering events is crucial but not straightforward. Based on the existing uncertainties and available observation approaches, the following research questions have been identified:

- Which indices allow the detection of tree canopies in bloom from phenocam imagery?
- And at which spatial scales can flowering events be detected? Inherently, is it potentially possible to apply optical indices suitable to detect flowering in phenocam data as well as to apply it to satellite imagery?
- To what extent do temporal patterns of drought events explain the occurrence of flowering?  
Is drought a plausible trigger for mass flowering events?

To address these questions, phenocam and satellite data for a test site in Malaysian Borneo have been studied and results have been discussed in the framework of previous studies on general flowering.

## 2. General flowering

The unique reproductive phenology of Southeast Asian aseasonal tropical dipterocarp forests is characterised by general flowering, a community-wide synchronous flowering event on a supra-annual schedule (e.g. Ashton et al., 1988; Azmy et al., 2016; Nagai et al., 2016; Numata et al., 2003; Sakai et al., 1999, 2006).

Kurten et al. (2017) give a comprehensive overview of hypotheses that try to explain why general flowering is restricted to Southeast Asia. Janzen (1974) first formulated the hypothesis that general flowering and subsequent synchronised seed and fruit production satiates seed and seedling predators. A theory that research highly focuses on until this day. The evolutionary fitness benefit improves seedling survival (Curran & Webb, 2000; Kurten et al., 2017; Sakai et al., 2006; Sakai & Itioka, 2016; Sun et al., 2007). According to Janzen (1974), *Dipterocarpaceae*, particularly the main genera *Shorea*, evolved in Southeast Asia's tropical rainforest. This has since been proven false (Morley, 2000). Ashton et al. (1988) proposed an alternative hypothesis, theorising that *Dipterocarpaceae* have originated in Gondwana and spread over Southeast Asia after the convergence of the Indian subcontinent and Asia. During this time, they experienced aseasonally dry monsoonal climate, which became an aseasonal perhumid climate in the Miocene (Morley, 2000; Sakai et al., 2006). Therefore, general flowering would likely be the result of evolutionary conservatism (Kurten et al., 2017) of the *Dipterocarpaceae* that are physiologically trained to wait for a period of low precipitation as a trigger (Sakai et al., 2006). This is supported by findings of Kurten et al. (2017) who claim that species only flowering during general flowering events in tropical rainforests do so annually in seasonally dry climates. The annual flowering is preceded by the same climatic cues that are expected to be triggers for general flowering events.

General flowering events take place on a community level in the Southeast Asian rainforest (Brearley et al., 2007; Butt et al., 2015; Numata et al., 2003, 2013). Hundreds of plant species across taxonomic levels, including most dipterocarp trees but also shrubs and emergent trees (e.g. *Euphorbiaceae* and *Leguminaceae*) as well as epiphytic orchids, can synchronise flowering and fruiting events (Ashton et al., 1988; Sakai, 2002; Sakai et al., 1999, 2006; Sakai & Itioka, 2016). This synchronous reproduction increases seedling survival chances and is thus a fitness advantage compared to seasonal flowering and seed production (Chen et al., 2018). This fitness advantage may outweigh the demographic disadvantage of fewer reproductive opportunities.

General flowering events are, unlike other flowering events in equatorial rainforest, temporally and spatially irregular. Synchronous reproduction fluctuates highly between twice a year up to a return frequency of ten years (Ashton et al., 1988; Azmy et al., 2016; Chen et al., 2018; Janzen, 1974; Kurten et al., 2017; Moore et al., 2016; Numata et al., 2003, 2013; Sakai, 2002; Sakai et al.,

1999, 2006; Sakai & Itioka, 2016; Yasuda et al., 2003). Annual precipitation and temperature patterns, due to the monsoon activity's, make spring and autumn the most likely periods for general flowering (Azmy et al., 2016; Numata et al., 2003). In both cases, the total event has a time span of a few months (Numata et al., 2013; Sakai et al., 2006; Sakai & Itioka, 2016) due to the fact that not all species flower at the exact same time but within the same time period. This temporal variation, caused by the high biodiversity, results in species-specific phenological sensitivity to environmental cues (Chen et al., 2018; Nagai et al., 2016). Synchronization of these reproductive events occurs within but also between regions (Ashton et al., 1988; Azmy et al., 2016; Cannon et al., 2007; Numata et al., 2003, 2013; Yasuda et al., 1999). Nevertheless, the spatial scale, extent, and distribution of general flowering events is highly variable (Numata et al., 2013; Sakai et al., 2006).

## **2.1. Relevance**

General flowering is ecologically and socially relevant for the Southeast Asian tropical rainforests and, therefore, influences the management and conservation efforts. For example, it contributes significantly to the high diversity of the dipterocarp forest (Sakai & Itioka, 2016). Thus, identification of the trigger is crucial to determine the role of climatic conditions for phenology and to assess why no other tropical region experiences community-wide flowering events (Sakai et al., 2006). However, not only identifying the trigger but also generating detailed and accurate maps of the extent and intensity of general flowering events is crucial for management strategies (Wohlfart et al., 2014). To evaluate the ecosystem functions and their spatio-temporal variability, timing and patterns of plant phenological stages, such as leaf flush, leaf colouring, leaf fall, flowering, bud burst, mast seeding and fruit production must be monitored (Nagai et al., 2017; Richardson et al., 2013).

Extreme events can change the composition, structure and functioning of plant communities or an ecosystem (Figure 1; Harrison, 2001; Moore et al., 2016). Recent climate projections indicate an increase in frequency, intensity, and duration of climate extremes in the 21st century (Butt et al., 2015). With climate extremes being a likely trigger, general flowering and fruiting events in the tropics are likely to change significantly (Azmy et al., 2016; Butt et al., 2015).

As general flowering events are the only time of reproduction for some dipterocarp species, the alteration of such events due to climate change can have a significant impact on the forests' regeneration (Azmy et al., 2016; Numata et al., 2013; Sakai & Itioka, 2016). If the timing of flowering shifts, it may mismatch with the life cycles of pollinators providing critical ecosystem services (Butt et al., 2015; Fitchett et al., 2015; Nagai et al., 2017). This extends to vertebrate

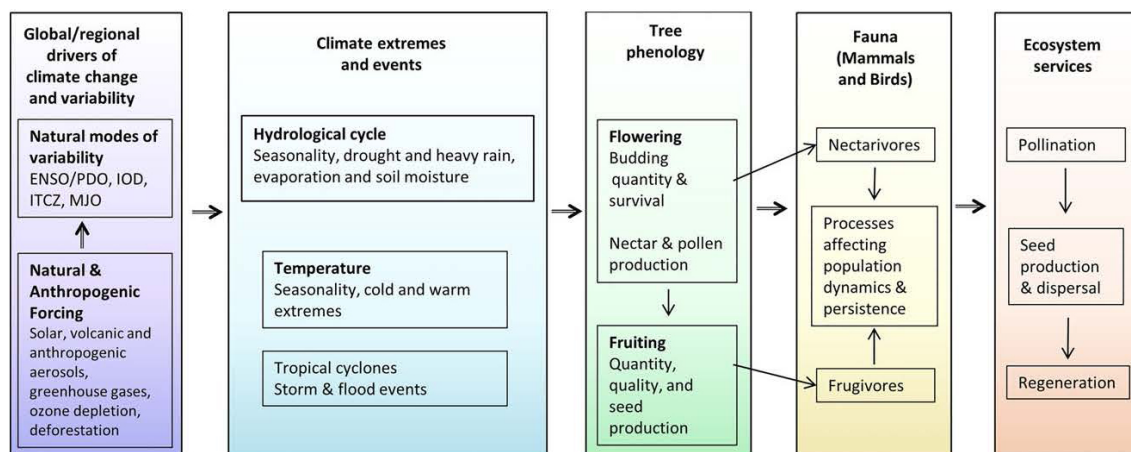


Fig. 1: The interaction between climate and weather extremes in tropical and subtropical regions and the impact on tree phenology and further impacts on dependent fauna and ecosystem functions. Natural variability in climate like El Niño-Southern Oscillation (ENSO), Pacific decadal oscillation (PDO), Indian Ocean Dipole (IOD), intertropical convergence zone (ITCZ) and Madden-Julian oscillation (MJO) are affected by natural and anthropogenic drivers. They can influence climate extremes through changes in the hydrological cycle, temperature regime and storm events. These in turn affect phenological events like flowering, budding and fruiting. Dependant nectar and fruit availability is vital for vertebrates. Further, ecosystem services like pollination, seed dispersal and forest regeneration depending on tree phenology might alter community composition and species' persistence. Schematic representation taken from Butt et al. (2015).

fauna (e.g. starlings (*Sturnidae spp.*), bearded pigs (*Sus barbatus*) as well as sun bears (*Helarctos malayanus*)) that obtain nectar or fruit as a key nutrient resource for building up reserves for non-mast years and are in turn crucial for seed dispersal (Butt et al., 2015). The complementary timings can affect reproduction and survival of flora and fauna and result in a total loss of biodiversity and disrupted ecosystem functions and services (Fitchett et al., 2015; Nagai et al., 2017).

Forest resources are economically important as export goods (Sakai & Itioka, 2016). Diptero-carp logs are of immense value to the global tropical hardwood trade and make up four fifth of Southeast Asia's timber export (Tito de Morais et al., 2015). Local people also depend on the forest resources as they collect wild fruits, harvest illipe nuts and honey, and hunt for wild boars (Sakai & Itioka, 2016).

## 2.2. Potential triggers

Most trees in temperate forests flower around the same time every year due to temperature thresholds or cumulative heat sums (Sakai et al., 2006). Flowering in equatorial forests in South America can be triggered by slight annual changes in both sunrise and sunset (Borchert et al., 2005). However, triggers and circumstances favourable for general flowering in Southeast Asia are not yet fully examined and understood, and, therefore, multiple controversial hypotheses exist (Sakai et al., 2006). Various plant taxa show similar flowering sequences during different general flowering events, supporting the hypothesis of a common environmental trigger. The trigger probably

consists of several dependent and irregularly occurring meteorological factors often associated with El Niño events (Ashton et al., 1988; Azmy et al., 2016; Cannon et al., 2007; Chen et al., 2018; Curran, 1999; Kurten et al., 2017; Sakai, 2002; Sakai et al., 2006; Yasuda et al., 1999; Yeoh et al., 2017). Namely, temperature drops (Ashton et al., 1988; Numata et al., 2003; Yasuda et al., 1999), periods of low precipitation (Appanah, 1985; Ashton et al., 1988; Brearley et al., 2007; Curran et al., 1999; Kobayashi et al., 2013; Medway, 1972; Numata et al., 2003, 2013; Sakai et al., 2006; van Schaik et al., 1993; Yasuda et al., 1999) and high solar radiation (Ng, 1977; van Schaik et al., 1993; Wycherley, 1973). Furthermore, stored nutrients have been mentioned as endogenous factors regulating general flowering events (Appanah, 1985; Burgess, 1972; Ichie & Nakagawa, 2013; Isagi et al., 1997; Sakai et al., 2006; Satake & Iwasa, 2000).

As mentioned above, droughts have often been put forward as the most likely trigger for general flowering events in Southeast Asia. The extent of some droughts seems to be related to the extent of general flowering (Numata et al., 2013). Sakai et al. (2006) have recorded droughts preceding all four general flowering events, although not every single flowering peak at Lambir Hills National Park, Sarawak, Malaysian Borneo, from 1993 until 2003. The time lag between the end of the drought and the flowering has been between four to ten days. Azmy et al. (2016) have measured significantly lower average precipitations before large-scale general flowerings. This suggests that the flowering intensity is affected negatively by preceding precipitation. Furthermore, they imply that the link between drought and general flowering may be more complex, as drought as a trigger may be more effective if followed by a warm, rainy period. RNA-Sequence studies of Kobayashi et al. (2013) found changing expression patterns in genes responsive to prolonged drought two weeks before flowering (Yamasaki et al., 2017). But droughts also have the potential to affect plant community composition by raising mortality rates among the vegetation (Delissio & Primack, 2003; Harrison, 2001). Nonetheless, defoliation and increased mortality of canopy trees improve the light conditions on the forest floor where seedling recruitment takes place (Sakai et al., 2006). Dry spells are favourable for pollination and resource accumulation, such as photosynthates – the dipterocarp trees' major carbon source for fruit development (Sakai et al., 2006; van Schaik et al., 1993). If a tree canopy is flowering or already carries fruit, extreme events such as severe and aseasonal droughts or heavy rain may cause flower or fruit fall (Butt et al., 2015). Severe droughts have recently been recorded more frequently, probably as a result of global warming (Harrison, 2001). If this trend continues, the forest composition and habitats may alter and a loss of biodiversity is likely to occur.

Ashton et al. (1988) identified temperature drops as the most plausible trigger for general flowering. These have later also been found to precede general flowering events (Numata et al., 2013;

Sakai et al., 1999; Yasuda et al., 1999). Azmy et al. (2016), however, did not find a significant difference in temperature before large and local scale general flowering events. On the contrary, they recorded a large temperature drop that was not followed by a general flowering event. Furthermore, temperature drops have not been recorded before every general flowering event (Sakai & Itioka, 2016). This raises the question if temperature drops can be considered as a trigger or if the combination with other circumstances may need to be considered. Synergistic effects of drought and lower temperatures have recently been found to trigger the activation of the flowering genes (Chen et al., 2018; Yeoh et al., 2017).

Increased radiation has also been mentioned as a possible trigger, but more recent studies (Azmy et al., 2016) did not support this. Azmy et al. (2016) indeed found a positive correlation between radiation and the magnitude and scale of a general flowering event, supporting the thesis that increased solar radiation may boost forest productivity (Brando et al., 2010). Rather than being a primary triggering factor, radiation can lead to resource accumulation and, therefore, relate to plant growth, photosynthetic activity, and vegetation cover (Huete et al., 2006; Azmy et al., 2016). Nutrient accumulation influences the magnitude in addition to the trigger's strength (Sakai et al., 2006) yet does not exclusively explain the timing of general flowering as suggested by Isagi et al. (1997).

## **2.3. Observing flowering events**

### **2.3.1. In-situ observations**

Phenological observations have been carried out in Kyoto as early as 801 A.D., where flowering dates have been noted in diaries and chronicles (Aono & Kazui, 2008). This historical record of annually recurring events for a particular species and location laid the foundation for ground-based observations and is still predominant for phenological data collection (Fitchett et al., 2015).

Ground-based observations can provide detailed information of temporal changes related to specific plants, species, or communities (Hufkens et al., 2012; Nagai et al., 2017; Rodriguez-Galiano et al., 2015). To monitor phenological timings and shifts within natural variability the records need to be long and continuous (Fitchett et al., 2015; Sonnentag et al., 2012). Continuous, daily records of several species are intensive in both human labour and cost (Alberton et al., 2017; Hufkens et al., 2012; Nagai et al., 2017; Rodriguez-Galiano et al., 2015). These typically limit the geographical area and spatial variability covered by phenological studies (Alberton et al., 2017; Azmy et al., 2016; Filippa et al., 2016; Nagai et al., 2017; Nijland et al., 2016; Numata et al., 2013). The observations are carried out by multiple individuals and thus limited by subjectivity reflecting personal interests, level of commitment, frequency of observations, applied methods

and the personal definition of various life cycle events (Fitchett et al., 2015; Hufkens et al., 2012; Nagai et al., 2017; Nijland et al., 2016; Sonnentag et al., 2012; Sparks et al., 2000).

Using multiple datasets, favourably from several sites, can bridge occasional data gaps in one record if unified and overcome much of the statistical noise from observational inconsistencies (Fitchett et al., 2015; Rodriguez-Galiano et al., 2015; Sparks et al., 2000). To resolve the various drawbacks of in-situ observations, digital cameras, spectral radiometers, unmanned aerial vehicles, aircrafts, and satellites are used (Morisette et al., 2009; Nagai et al., 2018). However, ground-based observations are still needed to validate remote sensing observations (Azmy et al., 2016).

### **2.3.2. Phenocam imagery**

More recently, the use of digital cameras to monitor the environment globally has become more frequent and started to alter the way phenological data is collected (Alberton et al., 2017). Near-surface phenology at local scales (Böttcher et al., 2016; Hufkens et al., 2012) is monitored with so called phenocams which are commercial cameras that take repeated digital photographs (Sonnentag et al., 2012). This is also called near surface remote sensing (Fitchett et al., 2015).

Phenocam datasets provide information about the responsiveness, vulnerability, and resilience of ecosystems, their functions and services, land-use changes (e.g. deforestation, restoration processes), disturbances (e.g. fire, flood), and species invasion related to changes in climate (Alberton et al., 2017; Nagai et al., 2016). This information is used in landscape management and biodiversity conservation efforts at several scales (Alberton et al., 2017). Digital repeat photography addresses the shortfalls of both ground-based in-situ observations and satellite-derived remote sensing data and can bridge the gap between them (Alberton et al., 2017; Browning et al., 2017; Fitchett et al., 2015; Morisette et al., 2009). The images provide tremendous potential as reliable tools for various ecological applications, in particular when combined with ground-based observations and satellite images. E.g. it can serve as ground-truth to validate and interpret satellite remote sensing observations (Böttcher et al., 2016; Hufkens et al., 2012; Nagai et al., 2016). The archives of phenological images are growing and becoming important data sources for phenological research (Sonnentag et al., 2012).

### **2.3.3. Satellite imagery**

Satellite images show the spatial distribution of ecosystems (Nasahara & Nagai, 2015). When combined to a series of images, dynamics (i.e. temporal changes) of the ecosystem can be revealed. Thus, satellite remote sensing imagery provides valuable information for scientists. Since

the opening of the Landsat data archive in 2009 and the open access Sentinel Hub, the application of satellite remote sensing observations in environmental research has increased again (Azmy et al., 2016). Multi-decadal records became affordable and easily accessible. New data is provided continuously, allowing near real-time environmental observations (Lu & Hamunela, 2016).

Satellite derived remote sensing imagery rapidly advanced the understanding of global phenology (Yamasaki et al., 2017). Large geographic areas can be monitored simultaneously and provide, if consistent, valuable data for environmental studies such as agricultural development, food security, forest management, biodiversity monitoring, numerical weather predications, and climate modelling (Brown et al., 2017; Park & Miura, 2011). The fusion of high spatial and high temporal remote sensing data can overcome problems such as the delineation of the mixed pixels due to the vegetation's heterogeneity (Liu et al., 2017; Wohlfart et al., 2014).

### 3. Study site

The data used in this study was collected at Lambir Hills National Park (LHNP) in Sarawak, Malaysian Borneo ( $4^{\circ}11'44''\text{N}$ ,  $114^{\circ}02'26''\text{E}$ ; Figure 2). The study site is a core site of the University of Zurich Research Priority Program (URPP) on Global Change and Biodiversity and of ESA's GlobDiversity project. Southeast Asia and especially Borneo is home to some of the world's biodiversity hotspots and its forests include highly diverse tree communities (Tito de Morais et al., 2015). Nevertheless, the region suffers from high annual deforestation, logging, and degradation rates due to increasing human population and socio-economic alterations (Wohlfart et al., 2014).

#### 3.1. Site characteristics

The study site is situated in a typical lowland mixed dipterocarp forest about 150 to 200 m above sea level (Ashton & Hall, 1992, Lee et al., 2002). LHNP, as part of Southeast Asia's tropical evergreen broadleaf rain forest, hosts the highest tree species diversity (1173 tree species on a 52ha plot) found on earth (Lee et al., 2002), which evolved from the forests' old age and a favourable perhumid equatorial climate (Harrison, 2001). The dominant canopy and emergent tree species at



Fig. 2: The location of Lambir Hills National Park ( $4^{\circ}11'44''\text{N}$ ,  $114^{\circ}02'26''\text{E}$ ) in the province Sarawak in Malaysian Borneo.

LHNP is the family of *Dipterocarpaceae* (Lee et al., 2002; Sakai & Itioka, 2016, Tito de Morais et al., 2015) with *Shorea*, *Hopea*, *Dipterocarpus*, and *Vatica* being the main genera. In Bornean tropical rainforests, trees can reach heights up to 70 metres (Sakai & Itioka, 2016) and the mean crown width is 11m (Ashton & Hall, 1992). Unlike in mixed and deciduous forests, there is a lack of distinct colour changes at the canopy of tropical rainforests (Nagai et al., 2016). *Dipterocarpaceae* carry whitish green and yellowish flowers, reddish seeds, and brownish fruits. Flower sizes range from under two millimetres to a few centimetres (Tito de Morais et al., 2015).

The tree canopy at LHNP was observed from tree towers, walkways, and a crane tower belonging to the canopy observation system (Nagai et al., 2016; Sakai et al., 2006).

### **3.2. Climate regime**

LHNP lays in a zone of perhumid tropical climate with low seasonality (Harrison, 2001). Air temperature at LHNP does not show seasonal variation. Temperatures are generally high and range from a daily mean maximum of 32 °C to a minimum of 24 °C (Lee et al., 2002) with the highest monthly mean temperature in May (Ichie et al., 2004) and the lowest in January (Kurten et al., 2017). These temperatures will increase according to the Representative Concentration Pathways (RCPs) gas concentration trajectories, with a higher rate of change in warm extremes (Butt et al., 2015).

The monsoon climate patterns in Southeast Asia and frequent extreme events, such as floods and droughts, exhibit a strong spatio-temporal variability (Suepa et al., 2016). Annual precipitation at LHNP sums up to 3000 mm, with monthly mean rainfall >150 mm (Ichie et al., 2004; Lee et al., 2002). Minor droughts most often occur from February to March before the summer monsoon arrives from the Indian Ocean, or occasionally from August to September before the monsoon from the Pacific Ocean reaches Southeast Asia and depend on the movements of the intertropical convergence zone (Harrison, 2001). Periods of reduced precipitation or severe droughts associated with the cyclical El Niño Southern Oscillation occur with high interannual and interdecadal variability (Butt et al., 2015; Harrison, 2001). Sakai et al. (2006) noticed that droughts in this region mostly occurred during transition periods from La Niña to El Niño. According to Harrison (2001) droughts are becoming more severe and more frequent corresponding to a shift also indicated by RCP climate scenarios for dipterocarp forests in Southeast Asia (Butt et al., 2015).

The El Niño Southern Oscillation (ENSO) is one of the most important natural climate oscillations (Gebhardt et al., 2011) and causes significant natural disturbances (Harrison, 2001). Sea surface temperature anomalies in the central and eastern Pacific Ocean are linked with convection

cells and lead to alternations in the regional climate, including the occurrence of droughts. During an El Niño event, the typical upwelling of cold water in front of South America's eastern coastline is stopped by higher sea surface temperatures and the high-pressure area from the Malaysian Archipelago relocates over this area. This results in a pressure anomaly between the Pacific Ocean and Australia described by a strongly negative southern oscillation index. Meanwhile, the sea surface temperatures over Southeast Asia are lower and, therefore, less evaporation occurs (Harrison, 2001). Butt et al. (2015) concluded that projected changes in ocean warming rates will increase the severity and frequency of El Niño events.

## 4. Data & methods

General flowering events are important for the ecology and economy of Southeast Asia and are, hence, the subjects of ongoing research. Observation of phenological changes across different plant species over various temporal and spatial scales requires long and continuous datasets (Sonnentag et al., 2012). For Lambir Hills National Park a long and continuous dataset exists. Since 1993, biweekly in-situ observations have been conducted (Figure 3). Since 2009, daily phenocam imagery from two cameras of the Phenological Eyes Network has been added. At the beginning the phenocams worked only sporadically and data gaps diminish the dataset's continuity. Furthermore, satellite imagery at low (>30 m) to medium (2-30 m) spatial resolution is now freely available. This satellite imagery bears great potential in extending the spatial range of research projects.

### 4.1. In-situ data

At Lambir Hills National Park, the monitoring of 486 individual plants of 300 species in 56 families started in 1993 (Sakai & Itioka, 2016). The sampling of the plants is weighted toward larger plants (i.e. emergent and canopy trees) and thus does not directly reflect the number of individuals of each species (Sakai et al., 2006). The observations were conducted in the eight-hectare Canopy Biology Plot from the towers and walkways constructed by the Canopy Biology Program in Sarawak and along the waterfall trail from the Operation Raleigh Tower, a tree tower constructed by Operation Raleigh (Sakai et al., 1999). Eventually a crane was constructed and the four-hectare Crane Plot was added to the list (Sakai & Itioka, 2016). Later the Operation Raleigh Tower was removed, and the list changed again. There were further slight changes, plants were

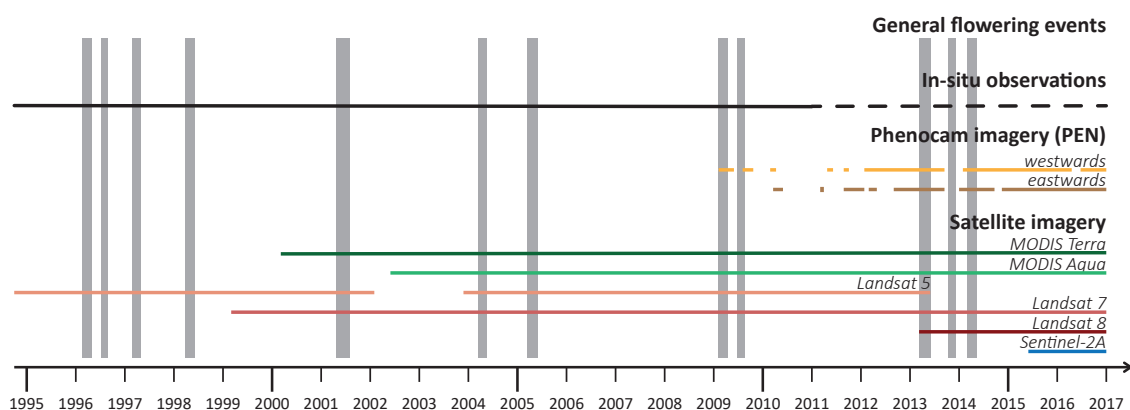


Fig. 3: General flowering events (grey bars) and visualised data availability at Lambir Hills National Park. In-situ observations have been acquired biweekly, two daily phenocam imagery datasets from the Phenological Eye Network (PEN) are available, and numerous satellite imagery is available for free at varying spatial and temporal resolutions. MODIS on board of Terra and Aqua provides daily coverage at 250m/500m/1km. The Landsat satellites deliver global coverage every 16 days at 30m spatial resolution with a 15m panchromatic band for Landsat 7 and Landsat 8. The twin mission with the satellites Sentinel-2A and Sentinel-2B (launched in 2017) provides a combined global coverage within five days at 10m/20m/60m.

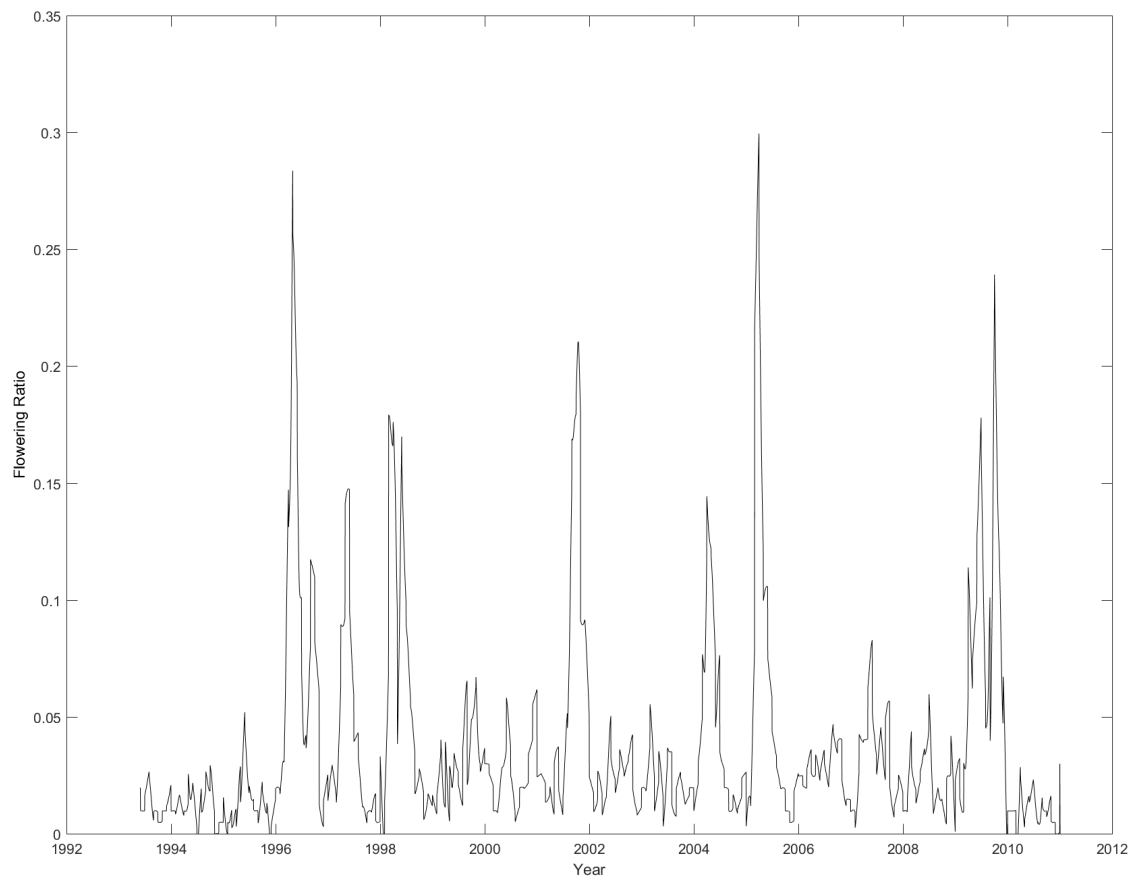


Fig. 4: Flowering ratio – The proportion of flowering individuals out of 207 observed canopy plants in total. Biweekly in-situ observations collected over the time span of 18 years at Lambir Hills National Park.

added or removed to the observation, as they emerged or died respectively and exchanged as the walkway routes altered. The staff of the Forest department is continuing with the observation of plants in the eight-hectare and four-hectare plots.

The fraction of flowering and fruiting plants to other plants (Figure 4) was very low (i.e. 0.02-0.05) during the first years of the monitoring (Sakai et al., 1999). In 1996, this was interrupted by a sharp increase of the flowering ratio. During this year there were even two flowering peaks and some plants flowered during both events. The flowering period of different species were staggered (Roubik et al., 2005) with a concentration in the period from March to May (Figure 5).

Sakai et al. (2006) defined the 1996 general flowering at Lambir Hills National Park as large general flowering with two peaks and noted smaller general flowering events in 1997, 1998, and 2001. From the flowering ratio in Figure 4 we see another small general flowering event in 2004, a large one in 2005 and a large flowering with two peaks in 2009.

These in-situ observations form perfect ground-truth data to validate phenocam or satellite remote sensing datasets. Unfortunately, the in-situ dataset has a data gap from January 2011 to

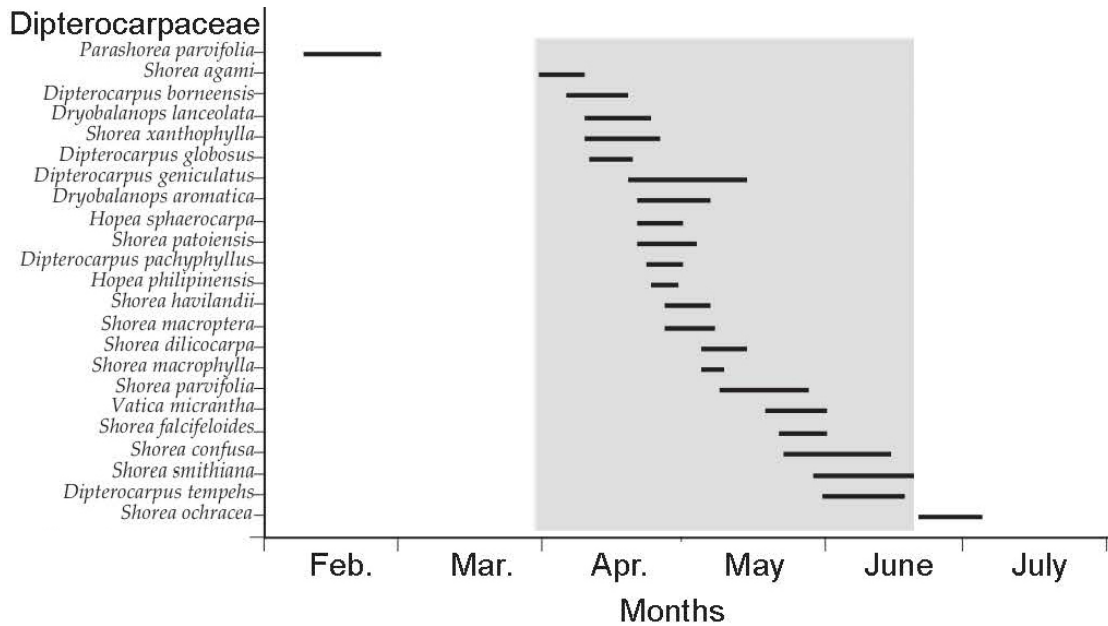


Fig. 5: Flowering periods of the canopy dominating Dipterocarpaceae family in Lambir Hills National Park during the general flowering of 1996. Data collected from the tree tower in Lambir Hills National Park by Roubik et al. (2005), figure taken from Sakai and Itioka (2016).

September 2014. The last general flowering event at Lambir Hills National Park was observed in April 2014 and is, therefore, not shown in the in-situ data.

#### 4.2. Phenocam imagery

Phenocams have been used a lot recently, mainly in the Northern Hemisphere covering deciduous forests (Alberton et al., 2017). The camera's field of view determines to which degree the data is representative of the landscape (Hufkens et al., 2012). Especially in the tropics, the use of hemispherical lenses (also called fish-eye lenses) can improve the selection of canopies with more precision and less covered area (Alberton et al., 2017). Near-noon images (i.e. between 11:00 and 13:00 local time) minimise the effects of shadowing and bidirectional reflectance distribution function (BRDF; Brown et al., 2017). Near-noon images are also best suited for comparisons with satellite products (Böttcher et al., 2016).

Phenocams are a low-cost investment and require low labour input for maintenance (Alberton et al., 2017; Brown et al., 2017; Fitchett et al., 2015; Nagai et al., 2016, 2018). Due to the small size, the cameras can easily be set up on instrumentation towers, at look-out points, or even underneath the canopy to monitor understory vegetation, with an oblique or horizontal view on the surrounding vegetation (Alberton et al., 2017; Browning et al., 2017; Fitchett et al., 2015; Hufkens et al., 2012; Sonnentag et al., 2012). The only requirement is a stable energy supply, otherwise fragmentary datasets will be the result. Phenocams provide long-term, continuous, near

remote phenological information on shoots, individual trees, multiple species, canopies, plant communities, landscapes and ecosystems (Alberton et al., 2017; Nagai et al., 2016). The data observations are in the form of quantitative monitoring of colour changes of the visible part of the electromagnetic spectrum with high, flexible spatial resolution for visual interpretation and automatic analysis (Alberton et al., 2017; Brown et al., 2017; Filippa et al., 2012; Nijland et al., 2016; Sonnentag et al., 2012). Simultaneous multi-site recording is possible. Recorded colour and brightness values depend on the illumination and viewing geometry as well as on shadowing effects, time of day, day of year, weather conditions and the plants' phenological cycle. Near-surface remote sensing happens at high temporal frequency and is more consistent than ground-based observations (Böttcher et al., 2016; Brown et al., 2017; Browning et al., 2017; Hufkens et al., 2012; Fitchett et al., 2015). Phenological images comprise a permanent record that can be analysed and re-checked, overcoming the subjectivity of ground-based observations. Phenocams are not affected by cloud cover and only minimally by atmospheric effects (Brown et al., 2017; Fitchett et al., 2015; Sonnentag et al., 2012). Rain, fog, haze, condensation and changing scene illumination affect the system instead. For normalising illumination alterations, a reference panel can be installed within the field of view of the camera.

#### **4.2.1. Phenological Eyes Network**

The imagery used in this thesis was collected by the Phenological Eyes Network (PEN; Nasahara & Nagai, 2015; Nagai et al., 2018). Since 2003, the network conducts long-term ground observations. The aim is to verify satellite remote sensing images of terrestrial ecosystems. Particularly, the PEN focuses on phenological changes in vegetation. Three different sensor types are used for the PEN sites: an Automatic Digital Fish-eye Camera (ADFC), a HemiSpherical SpectroRadiometer (HSSR), and a Sun Photometer (SP).

At Lambir Hills National Park, two ADFCs, consisting of a CoolPix 4500 digital camera (Nikon, Tokyo, Japan) and a FC-E8 fish-eye lens (Nikon), have been installed on the crane in water-proof containers (Nasahara & Nagai, 2015). The cameras are pointed sideways towards the west and east, 76 m above the ground – approximately 25-35 m above the canopy (Nagai et al., 2016, 2018). Both are solar powered and controlled remotely. The remote control used is often unstable and does not function continuously, resulting in data gaps (Nasahara & Nagai, 2015). The cameras take daily hemispherical 8-bit RGB images around noon local time (Nagai et al., 2016). But the timer gradually drifted from +0.11 to -0.22 min per day.

#### 4.2.2. Data preparation

As phenocam imagery is affected by rain, fog, haze, condensation, dirty lens and variation in scene illumination, the images had to be sorted first. In order to do so, Brown et al. (2017) used a three-day moving window and assigned the 90th percentile of an index value to the central image. But the images additionally contained non-canopy features interrupting the field of view on the canopy. Due to these numerous different factors that may render the images unsuitable (Figure 6), the sorting was done manually.

The installation of the cameras appeared to be not completely stable, in the sense that there were slight shifts in the cameras' field of view. To solve this, an adapted geometric transformation (estimateGeometricTransform) was conducted for every image using MATLAB (MathWorks, Natick (MA), USA) to align the image content. This allows a pixel-based analysis to extract within-ecosystem and within-individual phenological variability (Filippa et al., 2016).

Furthermore, due to the hemispherical lens the images are framed circularly and contain a part of the sky and the crane along with the tree canopy. Therefore, a region of interest (ROI) was defined and used as a mask for further analysis. The ROI was restricted to the images' foreground to minimise effects of atmospheric aerosols and low-lying clouds (Brown et al., 2017). Parts along the edge were also omitted due to distortion effects of the hemispherical lens. These criteria lead to a manual ROI definition of the representative area among the tree canopy in the foreground to minimise weather effects (Hufkens et al., 2012). The horizontal distance between trees and cameras ranges from about 10 to 100 m (Nagai et al., 2016). At greater distances, each tree is captured in fewer pixels than it would be closer to the camera and indices as well as spatial

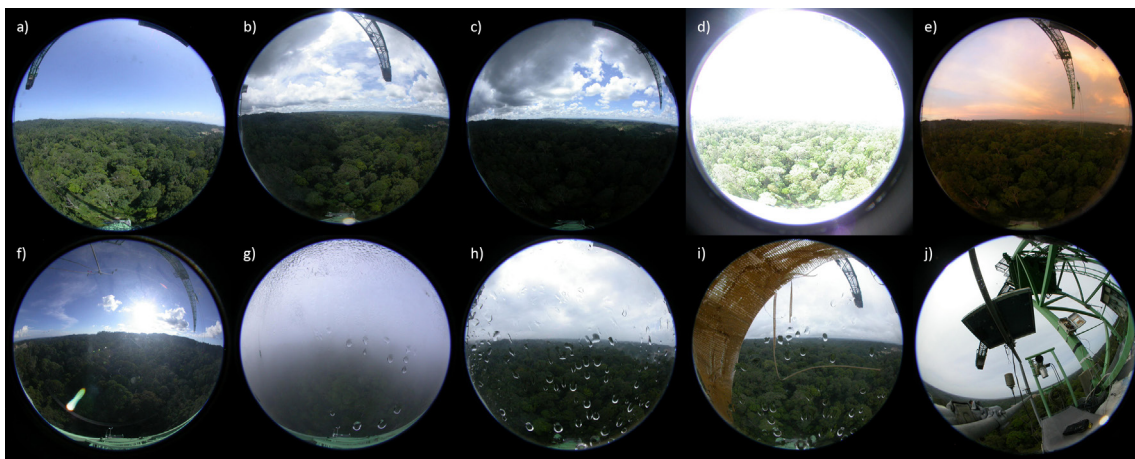


*Fig. 6: Selection representing the variation of the phenocam imagery from the Phenological Eyes Network: a) Sunny weather allows a perfect view on the canopy; b) Cloud shadows cover the canopy partially; c) The full camera's field of view lays in the shade; d) Overexposure; e) Image taken at dusk due to malfunctioning timer; f) Backlighting and lens flares; g) Fog; h) Condensation on lens; i) Loose building material hanging in front of the camera; j) The camera fell and the field of view changed totally. Data source see Section 4.2.1.*

metrics are affected by this. Therefore, the ROI was designed to contain tree canopies of similar sizes to ensure comparability.

Within the ROI, digital colour numbers were extracted, and different optical indices calculated. These were then tested whether they show and explain flowering patterns. More details on this can be found in Section 4.4.

### **4.3. Satellite data**

Time series derived from satellite imagery have been successfully applied in vegetation monitoring (Nijland et al., 2016). While satellite observations provide global coverage, they do so at various degrees of spatial and temporal resolution (Azmy et al., 2016; Hufkens et al., 2012; Nagai et al., 2017; Nijland et al., 2016; Rodriguez-Galiano et al., 2015; Suepa et al., 2016). The global coverage is especially important in order to study logistically challenging grounds and non-accessible regions (Cherrington et al., 2016; Fitchett et al., 2015). Single-point observations can be extended to representative landscape characteristics (Rodriguez-Galiano et al., 2015) and the trade-off between spatial and temporal resolution can be approached by integrating different sensors.

Satellite remote sensing cannot only provide multispectral and radiometric but also meteorological information (Azmy et al., 2016; Lu & Hamunyela, 2016). Climatological drivers of phenology occur on regional to global scale and, therefore, need broad coverage to be detected and analysed. Generally, both temporal and spatial resolution are coarser than for near-surface remote sensing data. Spatially and compositionally complex, heterogeneous vegetation generates mixed pixels when working with medium to coarse spatial resolution (Liu et al., 2017; Wohlfart et al., 2014). Satellite remote sensing is useful for observations of land surface phenology on regional to global scales but representativeness for phenological changes is limited on ecosystem or species-level (Filippa et al., 2016; Hufkens et al., 2012; Liu et al., 2017; Nagai et al., 2017). There is a trade-off between the two, higher spatial resolution (i.e. the level of spatial detail) usually entails coarser temporal resolution (i.e. revisit time) and vice-versa (Liu et al., 2017; Nijland et al., 2016). Cloud-contamination reduces the frequency of useable multispectral imagery especially in the tropics (Hufkens et al., 2012). Therefore, precise characterisation of rapid phenological processes, such as leaf emergence, are difficult to monitor (Nagai et al., 2017). The moderate-imaging resolution spectroradiometer (MODIS) provides daily coverage and is thus favourable for removing cloud contamination and allows advanced insights on temporal processes (Huete et al., 2006; Park & Miura, 2011). Additionally, noise in the satellite data and errors in processing methods increase uncertainty in land surface phenology analysis (Rodriguez-Galiano et al., 2015).

#### 4.3.1. Satellite imagery

Satellite imagery is an affordable and convenient way to look at the Earth's surface on a regional to global scale. Depending on the purpose, a high revisit frequency is favourable. This is provided by the Moderate Resolution Imaging Spectroradiometer (MODIS) instrument aboard both satellites Terra (launched 1999) and Aqua (launched 2002) of the U.S. National Aeronautics and Space Administration (NASA). The twin-MODIS design provides global coverage every one to two days (NASA, 2018a). The spatial resolution is 250 metres for bands 1-2, 500 metres for bands 3-7 and 1 kilometre for bands 8-36, including visible and infrared bands used for vegetation analysis. The moderate spatial resolution, however, make MODIS imagery a secondary candidate for the purpose of this study.

The Landsat family of satellites, among others, provide higher spatial resolution. NASA's Landsat 5, that carried the Multispectral Scanner System (MSS) and the Thematic Mapper (TM) instruments (NASA, 2018b) was launched in 1984 and delivered global land surface data for almost 29 years until the last command in 2013. Landsat 5 acquired global coverage of the Earth every 16 days at 30 metres spatial resolution in visible as well as in infrared wavelengths. The same temporal and spatial resolution apply to Landsat 7, launched in 1999 (NASA, 2018c) with the Enhanced Thematic Mapper Plus (ETM+). An additional panchromatic band at 15 metres enhances the spatial resolution. The imagery of Landsat 7 has data gaps between scan lines due to the malfunction of its scan line corrector (SLC). Landsat 8 was launched in February 2013 with the two instruments Operational Land Imager (OLI) and Thermal Infrared Sensor (TIRS) on board (NASA, 2018d) and was developed to continue long term observation records and improve older Landsat sensors regarding radiometric resolution (Liu et al., 2017). The bands within the visible, near-infrared and short-wave infrared, wavelengths are at a spatial resolution of 30 metres, the panchromatic band at 15 metres and the thermal band at 100 metres.

Higher spatial and temporal resolution is required for phenology analysis in order to not miss abrupt changes to the next phenological state of individual plants to communities. The twin mission Sentinel-2 by the European Space Agency (ESA) launched Sentinel-2A in 2015 and Sentinel-2B in 2017 (ESA, 2018). The identical satellites carry the Multispectral Imager (MSI) instrument that covers four visible and near-infrared bands at 10 metres spatial resolution, six red-edge/shortwave-infrared bands at 20 metres and 3 atmospheric correction bands at 60 metres. Full global coverage can be provided from combined Sentinel-2A and Sentinel-2B imagery every five days. The bands in the red-edge region, the short revisit time and the higher spatial resolution compared to Landsat satellites, bears high potential to improve the acquisition of time series monitoring vegetation (Chang & Shoshany, 2016; Malenovsky et al., 2016).

Using the Google Earth Engine (GEE; Gorelick et al., 2017), we computed surface reflectance time series of Landsat 5, 7, 8, and Sentinel-2 for the study site at Lambir Hills National Park. An advanced cloud and cloud shadows masking algorithm was applied. From these time series optical indices and their statistics were computed.

#### **4.3.2. Precipitation Measurement Missions**

Traditional weather stations only measure pointwise and do not reflect the spatial variation of rainfall. Satellite remote sensing is able to solve this problem and provide continuous and repeated precipitation data (Alexakis & Tsanis, 2016). Azmy et al. (2016) found that the results of remote sensing climate monitoring were consistent with data from meteorological stations.

The Precipitation Measurement Missions (PMM) by NASA and the Japan Aerospace Exploration Agency (JAXA) aimed to study precipitation for climate research. The Tropical Rainfall Measuring Mission (TRMM) satellite was launched in 1997 and ended its data collection in April 2015 (NASA, 2018e). The five instruments Precipitation Radar (PR), TRMM Microwave Imager (TMI), Visible and InfraRed Scanner (VIRS), Cloud and Earth Radiant Energy Sensor (CERES), and Lightning Imaging Sensor (LIS) collect weather data. Based on the success of the TRMM, the Global Precipitation Measurement (GPM) mission was initiated by NASA and JAXA (NASA, 2018f). The GPM mission comprises multiple satellites from international space agencies to extend the rainfall data collected by the TRMM satellite. The multi-satellite 3B42\*/TMPA product consists of three-hourly rainfall data between 50°N and 50°S at a 0.25° spatial resolution (Suepa et al., 2016; Yan et al., 2017). This data was transformed to daily precipitation measurements to reduce data size.

#### **4.4. Flowering metrics**

Phenological information can be extracted from the colour information of time series originating from digital photographs (Moore et al., 2016; Nasahara & Nagai, 2015). Vegetation indices, characterising the balance of red, green, blue and optionally near-infrared (NIR), can pick up processes and transition dates of phenology (Cherrington et al., 2016). Quantitative indices closely track colour changes of the vegetation canopy, such as canopy greenness, and can, therefore, indicate the plant development stage in various ecosystems (Moore et al., 2016). However, which index is most suitable to detect flowering may alter among tree species due to differences in the flower and leaf characteristics (Nagai et al., 2016).

#### 4.4.1. Red-edge indices

The normalized difference vegetation index (NDVI; Tucker 1979) is the most commonly applied red edge vegetation index. It is defined as:

$$NDVI = \frac{NIR-red}{NIR+red} \quad (1)$$

with NIR and red being the surface reflectance of near-infrared and red wavelengths (Park & Miura, 2011). These wavelengths are less prone to atmospheric scattering and are thus useful when working with satellite images (Reid et al., 2016). Nonetheless, NDVI is subject to saturation problems at moderate to high vegetation densities (Huete et al., 2002) due to the high absorption coefficient of chlorophyll in the red-edge region from 700-740nm (Chang & Shoshany, 2016). At close range, NDVI is outperformed by vegetation indices using the visible light spectrum (red, green, and blue) when assessing vegetation cover and condition (Reid et al., 2016). Nagai et al. (2014, 2016) did not detect seasonality in evergreen forests using NDVI.

Another index to improve the sensitivity in dense vegetation is the enhanced vegetation index (EVI; Huete et al., 2002) defined as:

$$EVI = G * \frac{NIR-red}{NIR+(C1*red-C2*blue)+L} \quad (2)$$

with NIR, red and blue being the surface reflectance. The blue band is used in the formula for atmospheric corrections (Park & Miura, 2011; Suepa et al., 2016). Additionally, the gain factor G, the coefficients of the aerosol resistance term C1 and C2 to reduce the impact of smoke from biomass burning, as well as the canopy background adjustment term L are used. For MODIS-EVI the terms are adopted as follows G = 2.5, C1 = 6, C2 = 7.5, and L = 1. In tropical wet evergreen vegetation with little seasonal variation, a constantly high EVI has been found (Moore et al, 2016; Nagai et al., 2014, 2016; Park & Miura, 2011).

#### 4.4.2. Visible-light indices

Indices calculated from visible light wavelengths in contrast to red-edge indices do not rely on infra-red measurements and are, therefore, applicable to not only satellite imagery but also to phenocam imagery without additional near-infrared data. Such an optical index is the green-red vegetation index (GRVI; Motohoka et al., 2010; Tucker 1979):

$$GRVI = \frac{green-red}{green+red} \quad (3)$$

which is simple to interpret in various ground covers using the visible green and red surface reflectance. GRVI can fall below zero when trees are bare or when the leaves change colour. Thus,  $GRVI = 0$  is a site-independent threshold for leaf green-up and the middle phase of autumn colouring of leaves. Furthermore, GRVI is sensible for subtle disturbances within an ecosystem and characteristic for different ecosystems. Nagai et al. (2012) found that GRVI detected phenology of evergreen trees, where NDVI and EVI were insensitive. Thus, GRVI might be more suitable for interannual and seasonal variability detection in tropical forests rather than other vegetation indices working with near-infrared wavelengths (Nagai et al., 2014). However, GRVI on the whole canopy did not detect temporal patterns of tree phenology in tropical forests (Nagai et al., 2016).

Chromaticity coordinates (CC) are numeric colour information that can also be used to analyse digital images and extract phenological information for any region of interest (Fitchett et al., 2015). The quantification of the colour information generates a vegetation index related to leaf colour representative for the vegetation's change in phenological status (Alberton et al., 2017; Moore et al., 2016; Nagai et al., 2016; Sonnentag et al., 2012). The timing of seasonal events like flowering, leaf expansion, and leaf fall of the canopy or of individual trees can be extracted (Moore et al., 2016; Nagai et al., 2016). CC are beneficial for or valuable in suppressing the effects of varying scene illumination for the RGB brightness levels (Brown et al., 2017; Gillespie et al., 1987; Nijland et al., 2014; Reid et al., 2016; Sonnentag et al., 2012; Woebbecke et al., 1995).

As the colour palette of *Dipterocarpaceae* ranges from whitish green and yellowish flowers to reddish seeds and brownish fruits, red chromatic coordinate (RCC, Gillespie et al., 1987) seemed to be most promising for flower detection within the tree canopies of Borneo's tropical rainforest (Eq. 4).

$$RCC = \frac{red}{red+green+blue} \quad (4)$$

There are two approaches how to compute a vegetation index on a ROI (Filippa et al., 2016). Either the index is calculated for each pixel and then averaged within a ROI, or each pixel within a ROI is analysed separately. We have decided to follow the ROI-averaged approach, because we wanted to look at scaling effects regarding the spatial resolution. First, we extracted the raw red, green and blue digital numbers from each pixel within the ROI and calculated their colour chromatic coordinates with the equation (4) and the respective green and blue chromatic coordinate equations. Then, pixelwise time-series were compiled for each year of the phenocam imagery. These time series were smoothed with a local regression using weighted linear least squares and a 2<sup>nd</sup> degree polynomial model assigning low weight to outliers. Then, the pixels were grouped in

differently sized ROIs and the mean for these ROIs was calculated. Afterwards, the mean of all ROI-averaged CC values and the variance between them was computed for each day.

#### 4.4.3. Observational scale

In diverse evergreen forests, specific phenological events such as leaf unfolding, flowering, fruiting, and leaf fall are species dependent and, therefore, spatially limited to single-tree canopies (Nijland et al., 2016). At broader scales, as for instance satellite pixels, mixed signals are recorded, and vegetation indices become continuous curves of indistinguishable signals from different species. Hufkens et al. (2012) noticed low covariance between vegetation indices extracted from satellite and camera data. The camera data reflected a small set of individual trees, whereas the satellite data represented the phenology of the larger landscape. The image analysis, hence, strongly depends on the defined ROI (Alberton et al., 2017). Sample sizes range from parts of a tree crown to individual trees over a portion of the canopy, a community profile to large landscapes. The detection of a tree crown in full bloom will be missed when calculating a vegetation index for the whole canopy.

The advantage of near-surface remote sensing is that the integration of multiple spatial scales by ROI selection is possible (Reid et al., 2016). The minimal mapping unit (MMU) of a digital camera image depends on the distance between the object and the lens. In the case of phenological

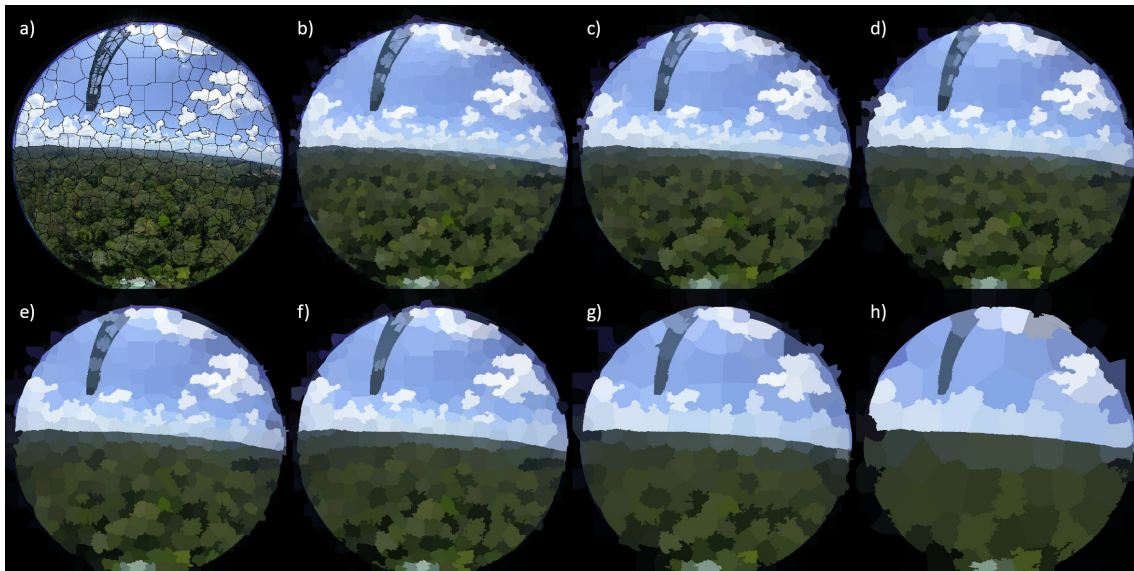


*Fig. 7: Region of interest sample sizes computed with the simple linear iterative clustering algorithm: a) Reference image with superpixel boundaries for clusters representing approximately an individual tree crown; b) The means of a very fine scale subdivision of tree crowns – shaded parts of the canopy are divided from illuminated parts; c) The means of a fine scale subdivision; d) The means of subdivision of tree crowns into two or three parts; e) The means of superpixels representing an individual tree crown; f) The means of two tree crowns; g) Of three tree crowns; h) And of approximately five tree crowns.*

imagery, single branches and parts of a tree can be distinguished. For a Landsat pixel, the MMU would be a community or around nine tree crowns in the tropical forests of Borneo, including some understory vegetation and forest floor, depending on the density of the canopy.

In order to identify the spatial scale at which flowering can be detected, we divided a reference phenocam image into three ROI sample sizes smaller than an individual tree crown (Figure 7, b-d), a sample size representing one individual tree crown (Figure 7, e), as well as sample sizes containing approximately two, three and five tree crowns, respectively (Figure 7, f-h). These ROIs were computed using the simple linear iterative clustering (SLIC) algorithm (Achanta et al., 2012). This superpixel algorithm groups pixels with similar values into regions and can thus catch the rounded forms of tree crowns rather than just segment the canopy into squares. Additionally, using this method background noise from other understory vegetation and other tree crowns as well as ground cover are minimised (Reid et al., 2016). CCs were then calculated for these different sample sizes. We have calculated the mean as well as the 90th percentile of the brightest pixels within the ROI.

#### 4.5. Quantification of dry periods

Droughts or dry periods have been named as likely trigger for general flowering events. However, the definition of drought varies among literature and general flowering studies (Numata et al., 2013). A compilation of definitions is listed in the following Table 1.

*Tab. 1: Varying drought definitions applied in literature and general flowering research in Southeast Asia.*

Total precipitation amount [mm]	Time period	Literature
< 100	30-days	Brunig (1969); Harrison (2001)
< 200	3-months	Azmy et al. (2016)
< 40	30-days	Sakai et al. (2006)
< 40	14-days	Kurten et al. (2017)
< 5	14-days	Ichie et al. (2004)

These tested thresholds were calculated and applied for the precipitation dataset, generated from the multi-satellite 3B42\*/TMPA product from the precipitation measurement missions. Then, correlations with general flowering events was analysed.

## 5. Results

First, the results from the CC analysis were presented, before further focus is laid on RCC and especially the variance of RCC measurements. Observational data was used for validation of peaks in RCC variance as a measurement of general flowering events. Then different observational scales were compared, before analysing the variance of RCC derived from satellite imagery. Furthermore, periods of low precipitation were compared to the timing of general flowering events. This chapter presents the results of these analyses in the mentioned order.

### 5.1. Chromaticity coordinates from the phenocam imagery

The chromatic coordinates proved effective at suppressing varying illumination, which is the case in the tropical lowland of Southeast Asia at Lambir Hills National Park. We, therefore, calculated red, green and blue chromatic coordinates from both datasets of the eastern and the western facing phenocam. The mean of the chromatic coordinates (Figure 8, a & c) did not show much variation,

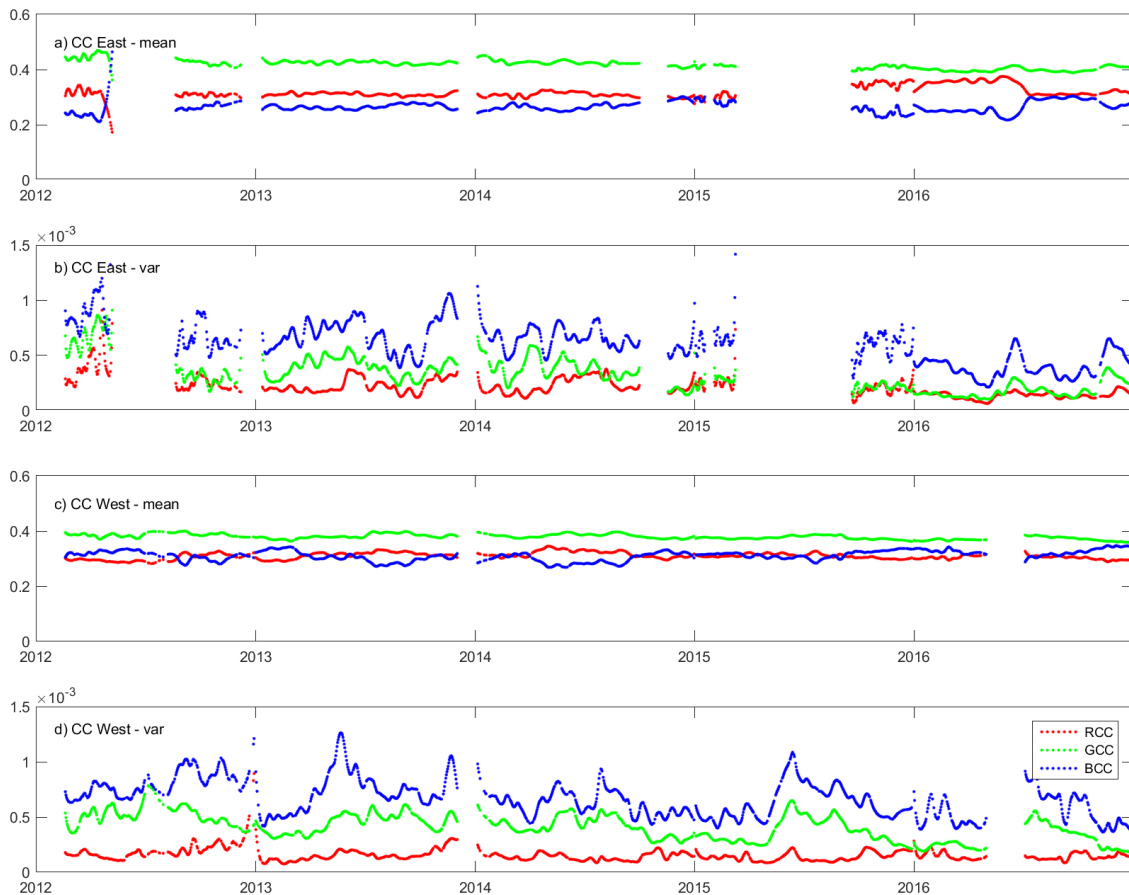


Fig. 8: RGB chromatic coordinates (CC): a) Mean values of the CC sampled over the smallest observational scale from the eastern facing camera; b) The variance of the CC between the sampled patches facing East; c) Mean values sampled over the smallest observational scale from the western facing camera; d) The variance of the CC between the sampled patches facing West.

although bigger differences between the values were extracted from the dataset from the eastern facing camera. Green chromatic coordinate has the highest values from the three CC. Blue light is lowest even though BCC and RCC are closer and change positions when looking at the western facing phenocam imagery. CC variance values (Figure 8, b & d) were more alternating with highest variance for BCC and lowest for RCC.

Due to the whitish green and yellowish flowers of the dominant canopy plant family of *Dipterocarpaceae*, RCC seems to be the most logical index to reveal flowering patterns. Therefore, further analysis focused on red chromatic coordinates.

The imagery of the digital camera facing West is more exhaustive, as the eastern dataset suffers from several data gaps. The longest data gaps are in 2012 and 2015 (Figure 8, a & b). Three smaller data gaps have been found at the end of 2012, at the end of 2013 and late in 2014 for the camera facing East. The gap at the end of 2013 also exists in the dataset from the camera facing West (Figure 8, c & d). An additional data gap in the middle of 2016 only affected the west-facing dataset.

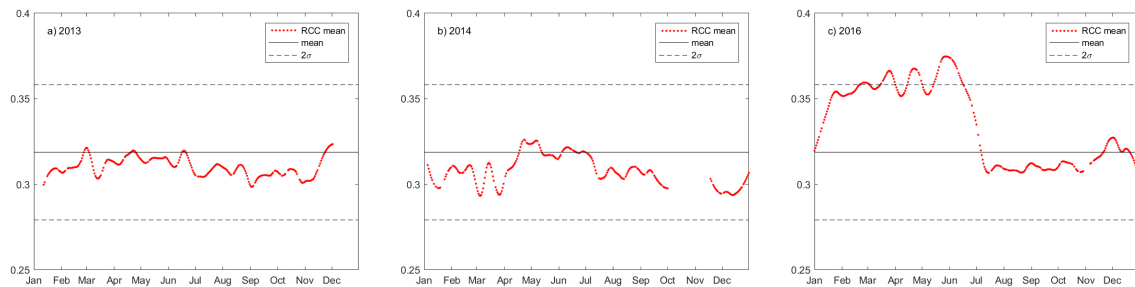


Fig. 9: The statistical mean (continuous line;  $0.3187$ ) and the range where 95% of the values lay within, defined by two standard deviations (dashed lines) from the mean of the red chromatic coordinates (RCC; red dots) from the smallest sample size. The statistics have been calculated for the years 2013 (a), 2014 (b), and 2016 (c) as relatively continuous datasets from the eastern facing camera are available for these years.

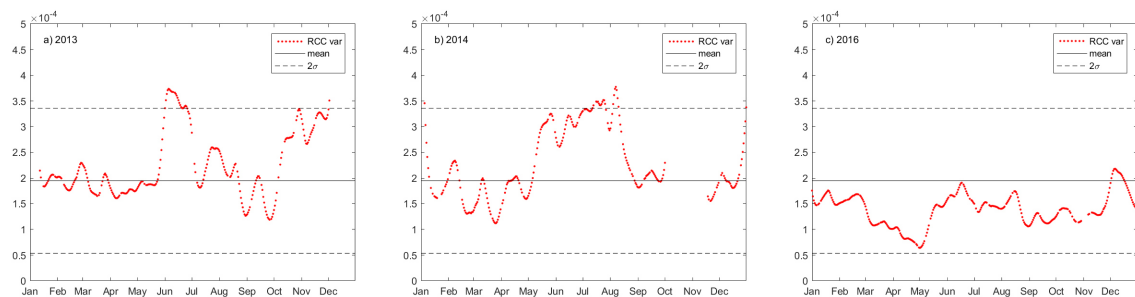


Fig. 10: The statistical mean (continuous line;  $1.9476 \cdot 10^{-4}$ ) and the range where 95% of the values lay within, defined by two standard deviations (dashed lines) from the variance of the red chromatic coordinates (RCC; red dots) from the smallest sample size. The statistics have been calculated for the years 2013 (a), 2014 (b), and 2016 (c) as relatively continuous datasets from the eastern facing camera are available for these years.

### 5.1.1. RCC mean

The RCC mean values from the smallest sample size were found to be around 0.32 (Figure 9). During the years 2013 and 2014, the values fluctuated slightly but they did not show any significant patterns. At the beginning of 2016, the RCC values increased and fluctuated around 0.36 for five months before the values dropped back down to the level of 2013 and 2014. During the second half of 2016, the lens was stained. No other hints for the rapid decrease were found when the phenocam images were inspected visually.

The RCC mean values did not show a significant correlation with the general flowering events in spring 2013, autumn 2013 and spring 2014.

### 5.1.2. RCC variance

The RCC variance usually alternated around  $2 \cdot 10^{-4}$  (Figure 10). This fluctuation was interrupted by a fast increase at the beginning of June 2013 and two slower inclines in October 2013 and May 2014. All these three peaks in the RCC variance noted deviations bigger than twice the standard deviation.

## 5.2. Validation

Validation with in-situ observations was, unfortunately, not possible, as the relevant years were missing in the available dataset. Alternatively, verification was done by visually comparing the amount of flowering tree canopies visible on the phenocam imagery. This qualitative validation showed an accumulation of trees in flower before and during the period where RCC variance was high.

Furthermore, Nagai et al. (2016) have marked flowering events from March to June 2013, August to September 2013, and May 2014. The first to change from green canopy to reddish green canopy was *Shorea beccariana* around the 16<sup>th</sup> of March 2013. Other trees of this species performed the same change around the middle of June. *Myristica gigantea* changed to a yellowish green canopy around the 17<sup>th</sup> of April, *Shorea ochracea* around the 24<sup>th</sup> of May, and *Shorea sp. cf. ovata* flowered around the 6<sup>th</sup> of June.

During the second flowering period, *Shorea beccariana* needed one week to develop full flowering on the 10<sup>th</sup> of August and the canopy changed from green to whitish green. *Swintonia acuta* developed whitish flowers over two weeks and peaked on the 22<sup>nd</sup> of August. *Shorea sp. cf. ovata* was partially covered with yellow flowers at the beginning of September.

Further canopy colour changes started to occur around the 29<sup>th</sup> of April 2014 when *Shorea curtisii* changed its canopy from green to yellowish green. *Crenolophon parvifolius* joined around

the 5<sup>th</sup> of May with reddish to yellowish hues, *Swintonia acuta* on the 9<sup>th</sup> of May and *Swintonia sp.* around the 10<sup>th</sup> of May in whitish colours, *Shorea ochracea* around the 23<sup>rd</sup> of June with reddish flowers, and *Shorea beccariana* added yellowish and reddish colours to the canopy at various times during May 2014 and July 2014. In August, *Shorea sp. cf. ovata* changed to a yellowish green canopy and more *Shorea ochracea* added reddish. Around the 7<sup>th</sup> of October *Myristica gigantea* dotted its green canopy with whitish flowers (Nagai et al., 2016).

### 5.3. Process scale of flowering

The variance of RCC varied depending on the sample size within the phenocam images. The highest variance was measured for ROIs smaller than the crown of one individual tree (Figure 11). The bigger the sample was in its spatial extent, the lower the RCC variance between the samples in one image. Several exceptions of the detected order occurred, but in general all the RCC variances followed the same temporal pattern.

This temporal pattern consisted of an up-and-down movement until the RCC variance values started to increase stronger in May. For the biggest observational size, the increase was slower and developed less steep than for smaller sample sizes.

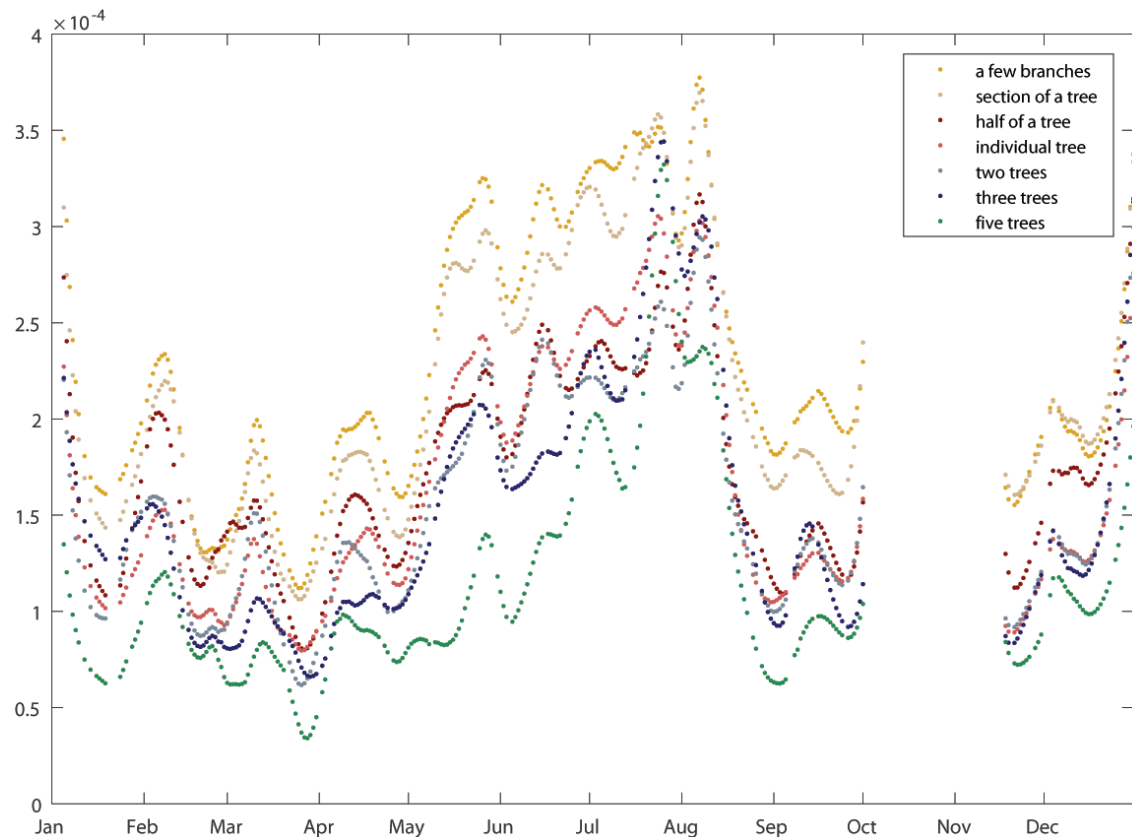


Fig. 11: The variance of red chromatic coordinates from the eastern facing phenocam at Lambir Hills National Park for 2014. The signals are sorted according to an observational scale from the smallest sample size representing a part of a tree canopy (approximately 2\*2m) to several trees in one sample (approximately 25\*25m).

Tab. 2: Different applied observational sample sizes from a region of interest representing a part of a tree canopy to several trees in one sample. And the highest red chromatic coordinate (RCC) variance between the samples in one image of the phenocam imagery facing East over the year 2014 as well as the date when the highest RCC variance value was measured.

Sample size	Highest RCC variance value [ $*10^{-4}$ ]	Date
A few branches	3.7743	07. August 2014
Section of a tree	3.6956	07. August 2014
Half of a tree	3.1670	07. August 2014
Individual tree	3.0536	24. July 2014
Two trees	2.9436	07. August 2014
Three trees	3.4414	26. July 2014
Five trees	3.3224	26. July 2014

the RCC variance values reached the maximum values. Afterwards, the variance values decreased within a month and fluctuated again.

The highest RCC variance values were reached at the end of July and the beginning of August (Table 2). The sample size containing approximately two tree crowns would have had its maximum at the end of the year. However, as the data gets anomalous in the second half of December, this period was not considered. The ROIs containing three to five tree crowns showed the highest variance at the 26<sup>th</sup> of July. The sample size for one tree had a smaller variance and reached its peak two days earlier. At all other observational scales, the peak was reached at the 7<sup>th</sup> of August and ranged from the lowest maximum variance of under  $3*10^{-4}$  (twotrees sample size) to the highest maximum RCC variance of almost  $3.8*10^{-4}$  for the smallest observational scale.

#### 5.4. Satellite time series

The imagery of Landsat 7, Landsat 8 and Sentinel-2A is available for free and provides imagery at 30-m and 10-m spatial resolution respectively at intervals of around two weeks. In the tropics of Southeast Asia, clouds are common and, therefore, less than the theoretical 23 images per year are available for analysis. After applying an advanced cloud filter, around ten images per year remained for each of the two Landsat satellites and six images for Sentinel-2A in 2016. For all three satellites the derived RCC variances over the whole area of Lambir Hills National Park (Figure 12, b - d) were higher than the RCC variance derived from the phenocam imagery (Figure 12, a).

The RCC variance derived from Landsat 7 imagery over the LHNP area (Figure 12, b) does show higher variance values during the mid-2013 general flowering event. Towards the end of 2013, slightly higher values were found as well as for the event in 2014. But then again, during

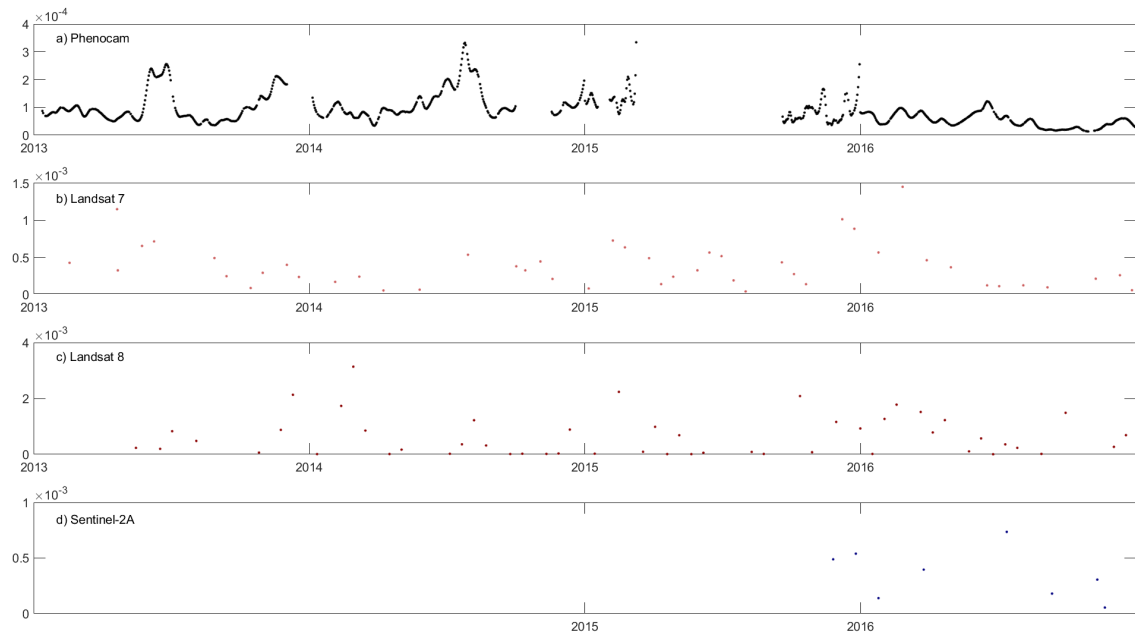


Fig. 12: Comparison of the RCC variance from the phenocam and satellite imagery. a) RCC variance of the eastern facing phenocam in Lambir Hills National Park (LHNP) over the biggest sample size (approximately 25\*25m); b) RCC variance derived over the whole LHNP area from cloud free Landsat 7 surface reflectance (SR) imagery, with a pixel size of 30\*30m; c) RCC variance derived over the whole LHNP area from cloud free Landsat 8 SR imagery, with a pixel size of 30\*30m; d) RCC variance derived over the whole LHNP area from cloud free Sentinel-2A top of atmosphere imagery, with a pixel size of 10\*10m.

2015 and the beginning of 2016, when no general flowering events occurred in this region, the RCC variance values fluctuated strongly and values were as high as during general flowering events.

When looking at the RCC variance values from the Landsat 8 imagery (Figure 12, c), peaks were found around the turn of the year 2013 to 2014, towards the beginning of the second half of 2014, the beginning of 2015, as well as from the end of 2015 to spring 2016. The first two peaks occurred during general flowering events, whereas the latter did not.

RCC variance values derived from Sentinel-2A imagery only exist starting from the end of 2015 onward. They do not follow a certain structure and, as there was no general flowering event since mid 2014, we could not compare the variance values from flowering periods to values from non-flowering periods.

### 5.5. Correlation of general flowering events and drought patterns

Two of the drought indices have shown a drought before the general flowering events in late July 2013. The indices defining total rainfall amount <100 mm for 30 continuous days (Figure 13, b), and <40 mm/14d (Figure 13, e) as drought events have marked dry periods at the end of June to the beginning of July. Drought conditions were only met for two days by the <100 mm/30d

threshold (Figure 13, b), but for two weeks by the  $<40$  mm/14d (Figure 13, e) threshold. The time lag between the recorded dry periods and the general flowering event was around three weeks. Before the general flowering event in early September 2013, only one index ( $<100$  mm/30d; Figure 13, b) showed a brief period where drought conditions were met. This period was at the end of July, approximately four to five weeks before the general flowering event. Drought was indicated by three indices before the event in April 2014. These three indices were  $<100$  mm/30d (Figure 13, b),  $<40$  mm/14d (Figure 13, e), and  $<5$  mm/14d (Figure 13, f), respectively. The droughts did occur in March and thus a few weeks before the general flowering event.

All three general flowering events were preceded by a drought when using the definition of total precipitation under 100 mm for 30 continuous days. On the other hand, this index showed many more periods of highly reduced precipitation, as did the other indices. Most droughts were detected by the  $<40$  mm/14d drought definition, least using  $<200$  mm/3m respectively. A particularly long drought occurred at the beginning of 2016 and was detected by all the used indices. The indices  $<100$  mm/30d and  $<40$  mm/14d observed a period of around four months with very little total rainfall amounts.

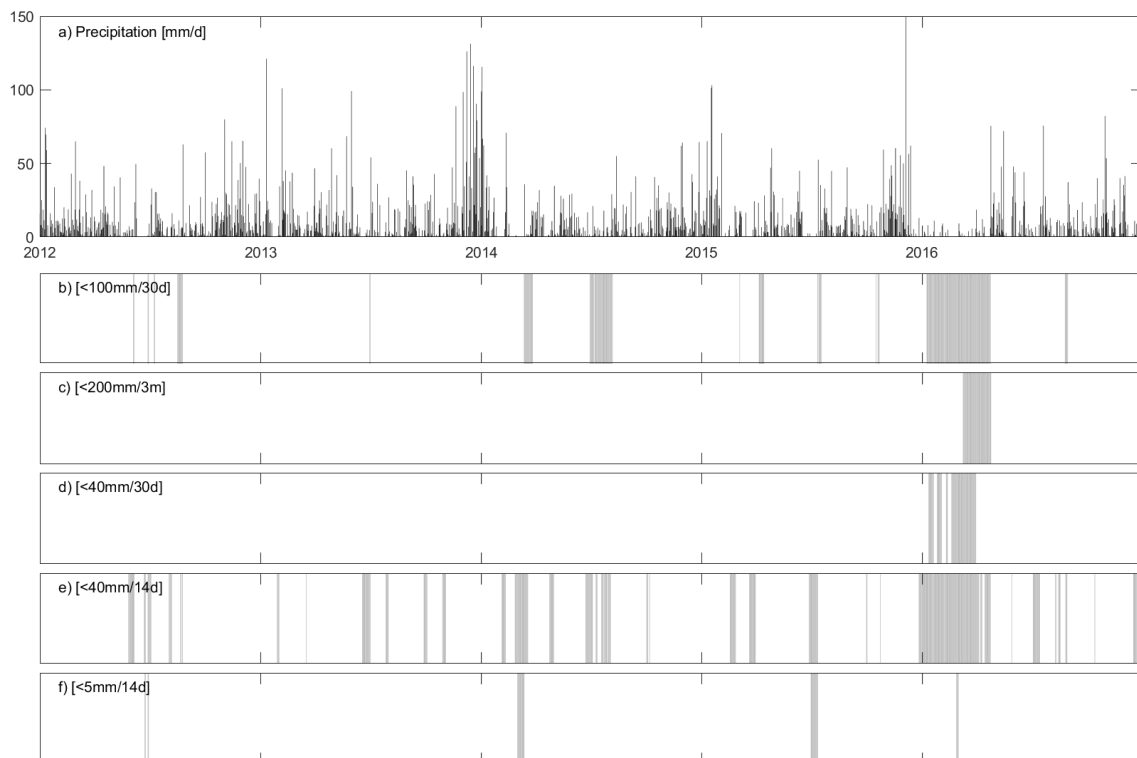


Fig. 13: Precipitation values and droughts at Lambir Hills National Park for the years 2012 to 2016: a) daily precipitation values from the PMM; b) periods with total rainfall amount  $<100$ mm for 30 continuous days (Brunig, 1969; Harrison, 2001); c) periods with total rainfall amount  $<200$ mm for 3 continuous months (Azmy et al., 2016); d) periods with total rainfall amount  $<40$ mm for 30 continuous days (Sakai et al., 2006); e) periods with total rainfall amount  $<40$ mm for 14 continuous days (Kurten et al., 2017); f) periods with total rainfall amount  $<5$ mm for 14 continuous days (Ichie et al., 2004).

## 6. Discussion

### 6.1. General flowering shown by Red Chromatic Coordinate

The red chromatic coordinate seems a promising optical index to discover whitish, yellowish and reddish flowers among the green tree canopy. When the flowers started to blossom, the green partially gave way to light colours with more reflectance within the red edge of the visible spectrum. When we looked at the RCC mean values, no clear pattern was visible, but there was a pattern for the RCC variance values.

The RCC variance values showed a correlation with recorded general flowering events at LHNP. All three peaks in the RCC variance values occurred approximately one to three months after the flowering of varying canopy tree species. With more different tree species flowering as it was the case in 2014, the increase in RCC variance values is slower but the peak itself is wider and variance values stay high for a three-month period. The two flowerings in 2013 showed high values for one or two months, respectively. This is probably due to the species involved in the respective flowering event. *Shorea beccariana* and *Shorea sp. cf. ovata* flowered during all three events but were joined by changing other species. The different tree canopy species do not flower at the exact same time but rather flower gradually (Ashton et al., 1988; Sakai & Itioka, 2016). Therefore, we found that the duration of general flowering events depends on the amount of different species involved in the particular event. Methodologically, we found that these events can be detected using RCC, in particular its variance, over an area of interest. This corresponds to the findings by Nagai et al. (2016) who found different RGB ratios and saturation values when comparing flowering and non-flowering individual trees.

The mean values fluctuated continuously with one exception. In the beginning of 2016, the values also showed an up-and-down movement but at a higher level. From a manual inspection of the phenocam images no hints were found for this phenomenon. When looking at the precipitation patterns, the reason for the increased RCC mean values became evident. The first half of 2016 was extremely dry. Droughts were detected by all applied indices and thresholds. During this period, the canopy was of a less lush green colour which in turn increases RCC values. This seems in line with the Alberton et al. (2017), who associated and explained daily changes in colour with daily measurements of climatic variables.

The available phenocam imagery featured several data gaps, especially in the dataset from the eastern facing camera. Still, we have used this dataset for a further analysis because the RCC variance calculated from the images facing East did show a correlation with general flowering events recorded at Lambir Hills National Park. The images from the western facing phenocam

did not provide such a link between the events and the calculated colour indices values. General guidelines for phenocam installation propose that the camera should face North when installed in the northern hemisphere and, subsequently, South when put up in the southern hemisphere. In this study, this was not available, and we therefore expect that detection accuracy can be improved. The cameras at LHNP were installed facing East and West. The sun appeared occasionally on the images causing backlighting and unbalanced light exposure. Nevertheless, it was more likely the reflection characteristics of the canopy causing the signal correlated with general flowering events to show up in one dataset but not the other. Cameras installed according to the general guidelines would also enable a more direct comparison to other studies concerned with general flowering events via phenocam imagery.

As the data gaps in 2012 and 2015 in the eastern facing imagery are four months long or bigger, these years were omitted for analysis. This also minimised the effects of the cameras' settings readjustments after resumption of work. With the data from 2013, 2014 and 2016 two years with three general flowering events and one year without an event were available. This constellation was biased towards years with the occurrence of general flowering event. This is unlikely as long-term records show long periods without general flowering events to be more probable. Therefore, signals of flower occurrence would be even more significant with longer datasets.

## **6.2. Links to leaf flushing and masting**

Other phenological events than general flowering like leaf flushing or masting might fall in line with flowering on a temporal scale.

### **6.2.1. Leaf flushing**

In tropical forests, leaf flushing occurs gradually throughout the year (Ichie et al., 2004; Nagai et al., 2014; Yan et al., 2017). However, large leaf flush such as starting from May 2016 at canopy scale can additionally be triggered by droughts and succeeding rainfall. During periods of severe water stress, a loss of old leaves with poor stomatal control occurs and when the resource is available again it comes to leaf flushing or flowering. Sakai et al. (2006) suggest that depending on the drought intensity buds produce either leaves or flowers. When producing leaves, RCC mean values will decrease, whereas green chromatic coordinate mean and variance values will increase in line with leaf flushing (Moore et al., 2016) as can be made out in Figure 9a. RCC variance values will increase (Figure 11c) with the leaf flushing. However, RCC values will additionally increase when flowers are produced. Due to the fact that not every tree species reacts the same, some might produce new leaves and other individuals will flower after a period with low precipitation. These

mixed signals could flatten out peaks in signals from flowering tree canopies.

Without in-situ reference data about the amount and the timing of leaf shedding and leaf flushing, disentangling the signals of new leaves and flowers will remain a challenge.

### **6.2.2. Masting**

After flowering events, the trees mast and produce seedlings and fruits. The seeds of *Dipterocarpaceae* are reddish and the fruits brownish. These colours may produce a stronger signal in the red chromatic coordinates compared to the whitish and yellowish flowers. Furthermore, Appanah (1985) stipulate that the fruits stay on the trees longer than the flowers do, as supported by Kurten et al. (2017). This minimises the effects of relatively small signals when the phenological cycles of individual species are gradually. Additionally, fruits are bigger in size and will, therefore, build a bigger portion of the signal from a ROI. Thus, fruits are more likely than flowers to show up in RCC measurements of the forest canopy, as a result explaining that the variance signal was strongest towards the end of the flowering and masting period. This seems in line with Appanah (1985), who measured a significantly higher percentage of trees with fruits, where the peak came four months after the flowering peak. Also, Brearley et al. (2007) observed fruit production following flowering by one to three months and continuing for up to three months after the completion of flowering. This time lag may need to be taken into account for remote-sensing based detection of general flowering events.

Keeping in mind that we observed a time lag between the flowering and the RCC variance peak values, we conclude that high RCC variance values are more sensitive to fruiting than to the flowering itself. However, fruiting depends on preceding flowering and the high RCC variance values can, therefore, be used as a proxy for flowering with an approximate time lag of one to three months.

Besides leaf flush and masting, other signals intermix in various ways. The mixing of signals from different trees during upscaling when analysing phenocam and satellite imagery is one way. But the measured signal can also be influenced by biological processes and circumstances such as the vegetation's state of health. Dry, dead and sick trees reflect a smaller proportion of green light (Reid et al., 2016), which in turn will raise the fraction of reflected red light and thus RCC values. Further influences from the atmosphere and the technical conditions of the imaging system bear additional potential to influence recorded signals. Comparability of graphical material is better the more homogeneous the image content is. In heterogeneous regions where vegetation types mix, comparing processes happening on different spatial scales turns out to be difficult. Phenological transition dates become inconsistent across scales (Liu et al., 2017).

### 6.3. Importance of the observational scale

Phenological observations are dependent on the pixel or ROI size, and the fraction of each component in that sample (Liu et al., 2017). The coarser the sample size the more likely mixed pixels are, e.g. under- and overstory vegetation or different plants next to each other. The more heterogeneous a sample is, the more difficult it is to extract a certain signal and compare it to measurements made at another spatial scale (Hufkens et al., 2012). Thus, the more trees are combined into one signal, the weaker the signal from each individual tree is. With the high biodiversity characteristic for this region, individual plant signals are concealed by averaging measurements over bigger ROIs. Furthermore, the different species do not flower simultaneously. Combined with the high heterogeneity it becomes even more crucial to work with fine scale data in terms of spatial resolution. The findings of Nagai et al. (2016) support this, as they did not detect temporal patterns in colour analysis of tree phenology over the whole canopy. In fact, results regarding flowering, leaf colouring, and leaf flushing were found when analysing individual trees.

Therefore, it is not surprising that the RCC variance signals behave differently for varying sample sizes. We found the signal for the smallest sample size to generally have the highest values. This was anticipated as small, spectrally similar patches became samples. This means that flowering parts of the tree canopy could be distinguished from non-flowering areas and thus a higher variance was found between the samples. The bigger the samples get, the more the signal gets mixed with background signals and thus concealed. This corresponds with the findings of Nagai et al. (2016) who did not detect any clear temporal patterns in colour values over the whole canopy but did do so when analysing individual trees. The slower and delayed increase for bigger samples in the variance signal do show this mixed signal problem. During the flowering, when trees flower according to a species and individual specific schedule, the variance within a sample would be high, whereas the variance between the samples did not yet increase for the biggest sample size. The signal builds up over time as more trees start to carry fruit and the heterogeneity within the sample decreases again. This is crucial for upscaling from the individual tree level to satellite pixel size. The biggest sample size applied in this research was approximately 25 m, slightly smaller than a Landsat-pixel and larger than a Sentinel-2 pixel. Hence, the sample size seems representative and a general flowering signal detection with satellite imagery should be possible. Section 6.5. provides more information on the possibilities of addressing general flowering via RCC variance signal with satellites.

The highest RCC variance signals in 2014 were found from the 24<sup>th</sup> of July to the 7<sup>th</sup> of August. For smaller sample sizes the peak was generally later than for bigger ones. The exception is the observational scale containing one individual tree per sample patch. In this curve, the peak was

reached the earliest. We do not know what caused this irregularity. Rather, we concluded that the fruit fall must occur over a certain period and does not happen simultaneously. This explains the maintained high and still raising variance values between smaller samples, whereas the variety for the bigger sample patches starts to decline earlier, as trees in various patches already start losing their fruit.

The maximum RCC variance signal was found to be highest for small sample patches and decreased with increasing patch size. The two biggest sample sizes that reach variance values as high as the values on sub-tree level formed an exception. A possible explanation could be the distribution of species. If the sample patches contain several similar trees within a patch the signal between the patches would be higher.

#### **6.4. Defining possible triggers**

The number of detected droughts varied greatly depending on the applied threshold from numerous droughts to almost none. It is, therefore, questionable how suitable those algorithms are for drought detection in Southeast Asia.

There were droughts of varying extent before each of the general flowering events during the period from 2012 to 2016. The time lag between the drought and the flowering ranged between three and five weeks. But none of the indices showed significant correlations. On the other hand, the large dry period at the beginning of 2016 was recorded as drought by all five applied indices. This drought was not followed by a general flowering event. This suggests that drought may not be a trigger for general flowering on its own. Rather, additional triggers like a temperature drop and resource accumulation in the vegetation are needed. The co-occurrence between other triggers and droughts might better correlate with the general flowering events.

As precipitation was the only climatic variable considered in this thesis, it is not possible to narrow down possible triggers for general flowering events. Furthermore, the analysis was only done for the area of the canopy biology plot in Lambir Hills National Park. Nevertheless, broad coverage of climatic variables is possible with satellite measurements (Azmy et al., 2016). Spatial extent of likely general flowering triggers, such as climatic variables, should be compared to the spatial extent of general flowering events, measured through daily colour changes (Alberton et al., 2017), to concentrate on dependencies.

#### **6.5. Outlook: satellite remote sensing**

The different observational scales applied during our research aimed at gradually upscaling the spatial resolution to the level of satellite imagery pixels. The largest sample size used is compa-

rable to a Landsat pixel. With this sample size, a signal related to general flowering could be detected. It must, therefore, be possible to catch the same signal with remote sensing observations. However, with bigger sample patches the signal was high over a shorter time period. Thus, detection of the signal during this shortened time span is the aim. With higher cloud density, the temporal resolution and, hence, the image density is much lower (Van Doninck & Tuomisto, 2017). Dipterocarp trees flower over a period of around two weeks which is already about the same as the temporal resolution of the Landsat satellites in the equatorial regions. Masked cloud contaminated pixels further lower the temporal resolution and a phenological event (e.g. general flowering) for individual trees can fall in between image acquisitions. Because the flowering events for the tree canopy of a region are longer than the event for an individual tree, there is still a signal to be picked up. Other than what we found, Brown et al. (2017) advised caution when comparing satellite derived signals to signals from phenocam imagery, as indices derived with an oblique angle at the vegetation tend to be greater than that observed from a near-nadir viewing geometry. With only a single or a few images during a general flowering event, the signal might get treated as an outlier and might then be lost when smoothing signals from satellite time series. If raw signals are used, errors stay within the dataset. The analysis of surface reflectance Landsat 7 and Landsat 8 data show higher values during general flowering events. But at other times, when no flowering occurred the RCC variance, values rose as high as they did during the events. Therefore, the detection of general flowering events seems to be impossible with Landsat imagery. Nevertheless, the imagery can be used to monitor the spatial extent of the phenomenon when other data sources (such as in-situ measurements or phenocam imagery) recorded an event.

For phenological analysis, daily satellite images would be best. Currently no such data set is available at a spatial resolution useful for flowering events of individual tree crowns. The 10-m pixel of the Sentinel-2 twin mission closely resembles the mean crown size and provides global coverage every five days. Also, the upscaling from phenocam imagery showed that 10-m pixels potentially show the signal. Since the launch of Sentinel-2A in 2015 and Sentinel-2B in 2017, there has not been a general flowering event in Lambir Hills National Park. We are curiously waiting for the next opportunity to test this hypothesis during an actual flowering event.

## 7. Conclusion

General flowering events are crucial for Southeast Asia. In order to find a way to detect them, we applied several optical indices on phenocam imagery, including chromaticity coordinates. Red chromatic coordinates (RCC) quantifies the proportion of red light to green and blue light from the visible wavelengths spectrum. The variance of RCC proved to be a measure allowing the flower detection from phenocam imagery.

Artificial upscaling on the phenocam imagery by grouping pixels of similar spectral characteristics to differently sized patches showed the effects of the observational scale. The largest sample patches resemble high spatial-resolution satellite imagery pixels. On this observational scale, a signal related to general flowering was still detected on phenocam imagery. It could not be isolated from Landsat 7 and Landsat 8 data but the higher spatial resolution of Sentinel-2 matches the detected observation scale and provides a very promising outlook for larger-scale mapping of general flowering.

Possible triggers for general flowerings are numerous named in the literature, with drought being the most likely trigger. Various drought definitions show different results for drought detection with satellite derived precipitation data. The drought indices applied did indicate the occurrence of general flowering events and provide a plausible trigger when combined with other climatic and biological factors.

## **8. Acknowledgments**

This research was supported and supervised by R. de Jong from the Remote Sensing Laboratories (RSL) at University of Zurich (UZH). We thank M. Schaepman from RSL, E. Yamasaki and K. Shimizu from the Department of Evolutionary Biology and Environmental Studies at UZH for providing insight and expertise greatly assisting the research. We would also like to show our gratitude to our colleagues from the RSL and the University Research Priority Programs for comments and insights from different perspectives. We greatly thank S. Nagai from the Yokohama Institute for Earth Sciences for providing us with the data from the Phenological Eyes Network. We thank I. Housman, K. Tenneson, C. Stam, M. Hancher and G. Donchyts who wrote parts of the Google Earth Engine code applied during this research. We are also immensely grateful to M. Luck for the assistance with programming, as well as J. Kesselring, I. Helfenstein and A. Gimmi for their comments on an earlier version of the manuscript.

## 9. References

- Achanta, R., Shaji, A., Smith, K., Lucchi, A., Fua, P., & Süsstrunk, S. (2012). SLIC Superpixels Compared to State-of-the-Art Superpixel Methods. *IEEE Transactions on Pattern Analysis and Machine Intelligence*, 34(11), 2274–2282.
- Alberton, B., Torres, R. da S., Cancian, L. F., Borges, B. D., Almeida, J., Mariano, G. C., dos Santos, J., & Morellato, L. P. C. (2017). Introducing digital cameras to monitor plant phenology in the tropics: applications for conservation. *Perspectives in Ecology and Conservation*.
- Alexakis, D. D., & Tsanis, I. K. (2016). Comparison of multiple linear regression and artificial neural network models for downscaling TRMM precipitation products using MODIS data. *Environmental Earth Sciences*, 75(14), 1077.
- Aono, Y., & Kazui, K. (2008). Phenological data series of cherry tree flowering in Kyoto, Japan, and its application to reconstruction of springtime temperatures since the 9th century. *International Journal of Climatology*, 28(7), 905–914.
- Appanah, S. (1985). General flowering in the climax rain forests of South-east Asia. *Journal of Tropical Ecology*, 1(03), 225–240.
- Ashton, P. S., Givnish, T. J., & Appanah, S. (1988). Staggered Flowering in the *Dipterocarpaceae*: New Insights Into Floral Induction and the Evolution of Mast Fruiting in the Aseasonal Tropics. *The American Naturalist*, 132(1), 44–66.
- Ashton, P. S., & Hall, P. (1992). Comparisons of Structure Among Mixed Dipterocarp Forests of North-Western Borneo. *The Journal of Ecology*, 80(3), 459–481.
- Azmy, M. M., Hashim, M., Numata, S., Hosaka, T., Supardi, N., Noor, M., & Fletcher, C. (2016). Satellite-based characterization of climatic conditions before large-scale general flowering events in Peninsular Malaysia. *Scientific Reports* 6, Article number: 32329.
- Borchert, R., Renner, S. S., Calle, Z., Navarrete, D., Tye, A., Gautier, L., Spichiger, R., & von Hildebrand, P. (2005). Photoperiodic induction of synchronous flowering near the Equator. *Nature*, 433(7026), 627–629.
- Böttcher, K., Härmä, P., Peltoniemi, M., Tanis, C. M., Aurela, M., & Arslan, A. N. (2016). Comparison of web-camera - and satellite-based observations on vegetation phenology in Finland. In *Agile 2016*. Helsinki, Finland.
- Brando, P. M., Goetz, S. J., Baccini, A., Nepstad, D. C., Beck, P. S. A., & Christman, M. C. (2010). Seasonal and interannual variability of climate and vegetation indices across the Amazon. *Proceedings of the National Academy of Sciences of the United States of America*, 107(33), 14685–14690.
- Brown, L. A., Dash, J., Ogutu, B. O., & Richardson, A. D. (2017). On the relationship between

- continuous measures of canopy greenness derived using near-surface remote sensing and satellite-derived vegetation products. *Agricultural and Forest Meteorology*, 247, 280–292.
- Browning, D., Karl, J., Morin, D., Richardson, A., & Tweedie, C. (2017). Phenocams Bridge the Gap between Field and Satellite Observations in an Arid Grassland Ecosystem. *Remote Sensing*, 9(10), 1071.
- Brunig, E. F. (1969). On the Seasonality of Droughts in the Lowlands of Sarawak (Borneo) (Über das jahreszeitliche Auftreten von Dürren im Tiefland von Sarawak (Borneo)). *Erdkunde. Erdkunde*.
- Burgess, P. F. (1972). Studies of the regeneration of the hill forests of the Malay Peninsula. *Malay For*, 35, 103–123.
- Butt, N., Seabrook, L., Maron, M., Law, B. S., Dawson, T. P., Syktus, J., & Mcalpine, C. A. (2015). Cascading effects of climate extremes on vertebrate fauna through changes to low-latitude tree flowering and fruiting phenology. *Global Change Biology*, 21(9).
- Cannon, C. H., Curran, L. M., Marshall, A. J., & Leighton, M. (2007). Long-term reproductive behaviour of woody plants across seven Bornean forest types in the Gunung Palung National Park (Indonesia): suprannual synchrony, temporal productivity and fruiting diversity. *Ecology Letters*, 10(10), 956–969.
- Chang, J., & Shoshany, M. (2016). Red-edge ratio Normalized Vegetation Index for remote estimation of green biomass. In 2016 IEEE International Geoscience and Remote Sensing Symposium (IGARSS) (pp. 1337–1339). IEEE.
- Chen, Y.-Y., Satake, A., Sun, I.-F., Kosugi, Y., Tani, M., Numata, S., Hubbell, S. P., Fletcher, C., Nur Supardi, Md. N., & Wright, S. J. (2018). Species-specific flowering cues among general flowering *Shorea* species at the Pasoh Research Forest, Malaysia. *Journal of Ecology*, 106(2), 586–598.
- Cherrington, E. A., Barbier, N., Ploton, P., Vincent, G., Sabatier, D., Berger, U., & Pelissier, R. (2016). Equatorial Forests Display Distinct Trends in Phenological Variation: A Time-Series Analysis of Vegetation Index Data from Three Continents. *IEEE Journal of Selected Topics in Applied Earth Observations and Remote Sensing*, 9(8), 3505–3511.
- Curran, L. M., Caniago, I., Paoli, G. D., Astianti, D., Kusneti, M., Leighton, M., Nirarita, C. E., & Haeruman, H. (1999). Impact of El Niño and Logging on Canopy Tree Recruitment in Borneo. *Science*, 286, 2184–2188.
- Curran, L. M., & Webb, C. O. (2000). Experimental tests of the spatiotemporal scale of seed predation in mast-fruiting *Dipterocarpaceae*. *Ecological Monographs*, 70(1), 129–148.
- Delissio, L. J., & Primack, R. B. (2003). The impact of drought on the population dynamics

- of canopy-tree seedlings in an aseasonal Malaysian rain forest. *Journal of Tropical Ecology*, 19(05), 489–500.
- Diez, J. M., Ibáñez, I., Miller-Rushing, A. J., Mazer, S. J., Crimmins, T. M., Crimmins, M. A., Bertelsen, C. D., & Inouye, D. W. (2012). Forecasting phenology: from species variability to community patterns. *Ecology Letters*, 15(6), 545–553.
- ESA. (2018). Satellite Description. Retrieved July 19, 2018, from <https://sentinel.esa.int/web/sentinel/missions/sentinel-2/satellite-description>
- Filippa, G., Cremonese, E., Migliavacca, M., Galvagno, M., Forkel, M., Wingate, L., Tomelleri, E., Morra di Cella, U., & Richardson, A. D. (2016). Phenopix: A R package for image-based vegetation phenology. *Agricultural and Forest Meteorology*, 220, 141–150.
- Fitchett, J. M., Grab, S. W., & Thompson, D. I. (2015). Plant phenology and climate change: Progress in methodological approaches and application. *Progress in Physical Geography*, 39(4), 460–482.
- Gebhardt, H., Glaser, R., Radtke, U., & Reuber, P. (2011). *Geographie: Physische Geographie und Humangeographie* (2. Auflage). Heidelberg: Spektrum Akademischer Verlag.
- Gillespie, A. R., Kahle, A. B., & Walker, R. E. (1987). Color enhancement of highly correlated images. II. Channel ratio and “chromaticity” transformation techniques. *Remote Sensing of Environment*, 22(3), 343–365.
- Gorelick, N., Hancher, M., Dixon, M., Ilyushchenko, S., Thau, D., & Moore, R. (2017). Google Earth Engine: Planetary-scale geospatial analysis for everyone. *Remote Sensing of Environment*, 202, 18–27.
- Harrison, R. D. (2001). Drought and the consequences of El Niño in Borneo: a case study of figs. *Population Ecology*, 43(1), 63–75.
- Huete, A., Didan, K., Miura, T., Rodriguez, E. ., Gao, X., & Ferreira, L. . (2002). Overview of the radiometric and biophysical performance of the MODIS vegetation indices. *Remote Sensing of Environment*, 83(1–2), 195–213.
- Huete, A. R., Didan, K., Shimabukuro, Y. E., Ratana, P., Saleska, S. R., Hutrya, L. R., Yang, W., Nemani, R. R., & Myneni, R. (2006). Amazon rainforests green-up with sunlight in dry season. *Geophysical Research Letters*, 33(6), L06405.
- Hufkens, K., Friedl, M., Sonnentag, O., Braswell, B. H., Milliman, T., & Richardson, A. D. (2012). Linking near-surface and satellite remote sensing measurements of deciduous broadleaf forest phenology. *Remote Sensing of Environment*, 117, 307–321.
- Ichie, T., Hiromi, T., Yoneda, R., Kamiya, K., Kohira, M., Ninomiya, I., & Ogino, K. (2004). Short-term drought causes synchronous leaf shedding and flushing in a lowland mixed dip-

- terocarp forest, Sarawak, Malaysia. *Journal of Tropical Ecology*, 20(06), 697–700.
- Ichie, T., & Nakagawa, M. (2013). Dynamics of mineral nutrient storage for mast reproduction in the tropical emergent tree *Dryobalanops aromatica*. *Ecological Research*, 28(2), 151–158.
- Isagi, Y., Sugimura, K., Sumida, A., & Ito, H. (1997). How Does Masting Happen and Synchronize? *Journal of Theoretical Biology*, 187(2), 231–239.
- Janzen, D. H. (1974). Tropical Blackwater Rivers, Animals, and Mast Fruiting by the *Dipterocarpaceae*. *Biotropica*, 6(2), 69.
- Kobayashi, M. J., Takeuchi, Y., Kenta, T., Kume, T., Diway, B., & Shimizu, K. K. (2013). Mass flowering of the tropical tree *Shorea beccariana* was preceded by expression changes in flowering and drought-responsive genes. *Molecular Ecology*, 22(18), 4767–4782.
- Kurten, E. L., Bunyavejchewin, S., & Davies, S. J. (2017). Phenology of a dipterocarp forest with seasonal drought: Insights into the origin of general flowering. *Journal of Ecology*, 106(1), 126–136.
- Lee, H. S., Davies, S. J., LaFrankie, J. V., Tan, S., Yamakura, T., Itoh, A., Ohkubo, T., & Ashton, P. S. (2002). Floristic and Structural Diversity of Mixed Dipterocarp Forest in Lambir Hills National Park, Sarawak, Malaysia. *Journal of Tropical Forest Science*. Forest Research Institute Malaysia.
- Lieth, H. (1974). Purposes of a Phenology Book (pp. 3–19). Springer, Berlin, Heidelberg.
- Liu, Y., Hill, M. J., Zhang, X., Wang, Z., Richardson, A. D., Hufkens, K., Filippa, G., Baldocchi, D. D., Ma, S., Verfaillie, J., Schaaf, C. B., & Liu, Y. (2017). Using data from Landsat, MODIS, VIIRS and PhenoCams to monitor the phenology of California oak/grass savanna and open grassland across spatial scales. *Agricultural and Forest Meteorology*, 237–238, 311–325.
- Lu, M., & Hamunyela, E. (2016). On-line Change Monitoring with Transformed Multi-Spectral Time Series, a Study Case in Tropical Forest. *The International Archives of Photogrammetry, Remote Sensing and Spatial Information Sciences*, 41, 987–989.
- Malenovský, Z., Homolová, L., Janoutová, R., Landier, L., Gastellu-Etchegorry, J. P., Berthelot, B., & Huck, A. (2016). Potential of the sentinel-2 red edge spectral bands for estimation of eco-physiological plant parameters. European Space Agency, (Special Publication) ESA SP, SP-740(May), 9–13.
- Medway, L. (1972). Phenology of a tropical rain forest in Malaya. *Biological Journal of the Linnean Society*, 4(2), 117–146.
- Moore, C. E., Brown, T., Keenan, T. F., Duursma, R. A., van Dijk, A. I. J. M., Beringer, J., Culvenor, D., Evans, B., Huete, A., Hutley, L. B., Maier, S., Restrepo-Coupe, N., Sonnentag, O., Specht, A., Taylor, J. R., van Gorsel, E., & Liddell, M. J. (2016). Australian vegetation

- phenology: new insights from satellite remote sensing and digital repeat photography. *Biogeosciences Discussions*, 1–30.
- Morisette, J. T., Richardson, A. D., Knapp, A. K., Fisher, J. I., Graham, E. A., Abatzoglou, J., Wilson, B. E., Breshears, D. D., Henebry, G. M., Hanes, J. M., & Liang, L. (2009). Tracking the rhythm of the seasons in the face of global change: phenological research in the 21st century. *Frontiers in Ecology and the Environment*, 7(5), 253–260.
- Morley, R. J. (2000). *Origin and evolution of tropical rain forests*. Origin and evolution of tropical rain forests. John Wiley & Sons.
- Nagai, S., Akitsu, T., Saitoh, T. M., Busey, R. C., Fukuzawa, K., Honda, Y., Ichie, T., Ide, R., Ikawa, H., Iwasaki, A., Iwao, K., Kajiwara, K., Kang, S., Kim, Y., Khoon, K. L., Kononov, A. V., Kosugi, Y., Maeda, T., Mamiya, W., Matsuoka, M., Maximov, T. C., Menzel, A., Miura, T., Mizunuma, T., Morozumi, T., Motohka, T., Muraoka, H., Nagano, H., Nakai, T., Nakaji, T., Oguma, H., Ohta, T., Ono, K., Pungga, R. A. S., Petrov, R. E., Sakai, R., Schunk, C., Sekikawa, S., Shakhmatov, R., Son, Y., Sugimoto, A., Suzuki, R., Takagi, K., Takanashi, S., Tei, S., Tsuchida, S., Yamamoto, H., Yamasaki, E., Yamashita, M., Yoon, T. K., Yoshida, T., Yoshimura, M., Yoshitake, S., Wilkinson, M., Wingate, L., & Nasahara, K. N. (2018). 8 million phenological and sky images from 29 ecosystems from the Arctic to the tropics: the Phenological Eyes Network. *Ecological Research*, 1–2.
- Nagai, S., Ichie, T., Yoneyama, A., Kobayashi, H., Inoue, T., Ishii, R., Suzuki, R., & Itioka, T. (2016). Usability of time-lapse digital camera images to detect characteristics of tree phenology in a tropical rainforest. *Ecological Informatics*, 32, 91–106.
- Nagai, S., Ishii, R., Suhaili, A. Bin, Kobayashi, H., Matsuoka, M., Ichie, T., Motohka, T., Kendawang, J. J., & Suzuki, R. (2014). Usability of noise-free daily satellite-observed green–red vegetation index values for monitoring ecosystem changes in Borneo. *International Journal of Remote Sensing*, 35(23), 7910–7926.
- Nagai, S., Saitoh, T. M., Kobayashi, H., Ishihara, M., Suzuki, R., Motohka, T., Nasahara, K. N., & Muraoka, H. (2012). In situ examination of the relationship between various vegetation indices and canopy phenology in an evergreen coniferous forest, Japan. *International Journal of Remote Sensing*, 33(19), 6202–6214.
- NASA. (2018a). GPM Mission Concept. Retrieved July 19, 2018, from <https://pmm.nasa.gov/gpm>
- NASA. (2018b). Landsat 5. Retrieved July 19, 2018, from <https://landsat.gsfc.nasa.gov/landsat-5/>
- NASA. (2018c). Landsat 7. Retrieved July 19, 2018, from <https://landsat.gsfc.nasa.gov/landsat-7/>
- NASA. (2018d). Landsat 8. Retrieved July 19, 2018, from <https://landsat.gsfc.nasa.gov/landsat-8/>

- data-continuity-mission/
- NASA. (2018e). MODIS Design. Retrieved July 19, 2018, from <https://modis.gsfc.nasa.gov/about/design.php>
- NASA. (2018f). TRMM - Tropical Measuring Mission. Retrieved July 19, 2018, from <https://trmm.gsfc.nasa.gov/>
- Nasahara, K. N., & Nagai, S. (2015). Review: Development of an in situ observation network for terrestrial ecological remote sensing: the Phenological Eyes Network (PEN). *Ecological Research*, 30(2), 211–223.
- Ng, F. S. P. (1977). Gregarious flowering of dipterocarps in Kepong, 1976. *Malaysian Forester*, 40(3), 126–137.
- Nijland, W., Bolton, D. K., Coops, N. C., & Stenhouse, G. (2016). Imaging phenology; scaling from camera plots to landscapes. *Remote Sensing of Environment*, 177, 13–20.
- Nijland, W., De Jong, R., De Jong, S. M., Wulder, M. A., Bater, C. W., & Coops, N. C. (2014). Monitoring plant condition and phenology using infrared sensitive consumer grade digital cameras. *Agricultural and Forest Meteorology*, 184, 98–106.
- Numata, S., Yasuda, M., Okuda, T., Kachi, N., & Noor, N. S. M. (2003). Temporal and Spatial Patterns of Mass Flowerings on the Malay Peninsula. *American Journal of Botany*. Botanical Society of America, Inc.
- Numata, S., Yasuda, M., Suzuki, R. O., Hosaka, T., Noor, N. S. M., Fletcher, C. D., & Hashim, M. (2013). Geographical Pattern and Environmental Correlates of Regional-Scale General Flowering in Peninsular Malaysia. *PLoS ONE*, 8(11), e79095.
- Park, S., & Miura, T. (2011). Moderate-resolution imaging spectroradiometer-based vegetation indices and their fidelity in the tropics. *Journal of Applied Remote Sensing*, 5(1).
- Pereira, H. M., Ferrier, S., Walters, M., Geller, G. N., Jongman, R. H. G., Scholes, R. J., Bruford, M. W., Brummitt, N., Butchart, S. H. M., Cardoso, A. C., Coops, N. C., Dulloo, E., Faith, D. P., Freyhof, J., Gregory, R. D., Heip, C., Höft, R., Hurtt, G., Jetz, W., Karp, D. S., McGeoch, M. A., Obura, D., Onoda, Y., Pettorelli, N., Reyers, B., Sayre, R., Scharlemann, J. P. W., Stuart, S. N., Turak, E., Walpole, M., & Wegmann, M. (2013). *Ecology. Essential biodiversity variables*. *Science (New York, N.Y.)*, 339(6117), 277–278.
- Reid, A. M., Chapman, W. K., Prescott, C. E., & Nijland, W. (2016). Using excess greenness and green chromatic coordinate colour indices from aerial images to assess lodgepole pine vigour, mortality and disease occurrence. *Forest Ecology and Management*, 374, 146–153.
- Richardson, A. D., Keenan, T. F., Migliavacca, M., Ryu, Y., Sonnentag, O., & Toomey, M. (2013). Climate change, phenology, and phenological control of vegetation feedbacks to the climate

- system. *Agricultural and Forest Meteorology*, 169, 156–173.
- Rodriguez-Galiano, V. F., Dash, J., & Atkinson, P. M. (2015). Intercomparison of satellite sensor land surface phenology and ground phenology in Europe. *Geophysical Research Letters*, 42(7), 2253–2260.
- Roubik, D. W., Sakai, S., & Gattesco, F. (2003). Canopy flowers and certainty: loose niches revisited. In *Arthropods of tropical forests: spatio-temporal dynamics and resource use in the canopy* (pp. 360–368). Cambridge: Cambridge University Press.
- Sakai, S. (2002). General flowering in lowland mixed dipterocarp forests of South-east Asia. *Biological Journal of the Linnean Society*, 75(2), 233–247.
- Sakai, S., Harrison, R. D., Momose, K., Kuraji, K., Nagamasu, H., Yasunari, T., Chong, L., & Nakashizuka, T. (2006). Irregular droughts trigger mass flowering in aseasonal tropical forests in asia. *American Journal of Botany*, 93(8), 1134–1139.
- Sakai, S., & Itioka, T. (2016). Long - term monitoring of plant reproductive phenology and observation of general flowering in Lambir Hills , Sarawak. In “Frontier in tropical forest research: progress in joint projects between the Forest Department Sarawak and the Japan Research Consortium for Tropical Forests in Sarawak (pp. 9–18).
- Sakai, S., Momose, K., Yumoto, T., Nagamitsu, T., Nagamasu, H., Hamid, A. A., & Nakashizuka, T. (1999). Plant Reproductive Phenology over Four Years Including an Episode of General Flowering in a Lowland Dipterocarp Forest, Sarawak, Malaysia. *American Journal of Botany*, 86(10), 1414.
- Satake, A., & Iwasa, Y. (2000). Pollen Coupling of Forest Trees: Forming Synchronized and Periodic Reproduction out of Chaos. *Journal of Theoretical Biology*, 203(2), 63–84.
- Schwartz, M. D. (2003). *Phenology: An Integrative Environmental Science (Second Edi)*. Springer.
- Sonnentag, O., Hufkens, K., Teshera-Sterne, C., Young, A. M., Friedl, M., Braswell, B. H., Milliman, T., O’Keefe, J., & Richardson, A. D. (2012). Digital repeat photography for phenological research in forest ecosystems. *Agricultural and Forest Meteorology*, 152, 159–177.
- Sparks, T. H., Jeffree, E. P., & Jeffree, C. E. (2000). An examination of the relationship between flowering times and temperature at the national scale using long-term phenological records from the UK. *International Journal of Biometeorology*, 44(2), 82–87.
- Suepa, T., Qi, J., Lawawirojwong, S., & Messina, J. P. (2016). Understanding spatio-temporal variation of vegetation phenology and rainfall seasonality in the monsoon Southeast Asia. *Environmental Research*, 147, 621–629.
- Sun, I.-F., Chen, Y.-Y., Hubbell, S. P., Wright, S. J., & Noor, N. S. M. (2007). Seed Predation Dur-

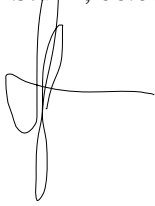
- ing General Flowering Events of Varying Magnitude in a Malaysian Rain Forest. *Journal of Ecology*. British Ecological Society.
- Tito de Moraes, C., Ghazoul, J., Maycock, C. R., Bagchi, R., Burslem, D. F. R. P., Khoo, E., Itoh, A., Nanami, S., Matsuyama, S., Finger, A., Ismail, S.A., & Kettle, C. J. (2015). Understanding local patterns of genetic diversity in dipterocarps using a multi-site, multi-species approach: Implications for forest management and restoration. *Forest Ecology and Management*, 356, 153–165.
- Tucker, C. J. (1979). Red and photographic infrared linear combinations for monitoring vegetation. *Remote Sensing of Environment*, 8(2), 127–150.
- Van Doninck, J., & Tuomisto, H. (2017). Influence of Compositing Criterion and Data Availability on Pixel-Based Landsat TM/ETM+ Image Compositing Over Amazonian Forests. *IEEE Journal of Selected Topics in Applied Earth Observations and Remote Sensing*, 10(3), 857–867.
- Van Schaik, C. P., Terborgh, J. W., & Wright, S. J. (1993). The Phenology of Tropical Forests: Adaptive Significance and Consequences for Primary Consumers\*. *Annu. Rev. Ecol. Syst.*, 24, 353–377.
- Woebbecke, D. M., Meyer, G. E., Von Bargen, K., & Mortensen, D. A. (1995). Color Indices for Weed Identification Under Various Soil, Residue, and Lighting Conditions. *Transactions of the ASAE*, 38(1), 259–269.
- Wohlfart, C., Wegmann, M., & Leimgruber, P. (2014). Mapping Threatened Dry Deciduous Dipterocarp Forest in South-East Asia for Conservation Management. *Tropical Conservation Science*, 7(4), 597–613.
- Wycheley, P. R. (1973). The phenology of plants in the humid tropics. *Micronesica*, 9(1), 75–96.
- Yamasaki, E., Altermatt, F., Cavender-Bares, J., Schuman, M. C., Garonna, I., Schneider, F. D., Guillén-Escribà, C., van Moorsel, S. J., Hahl, T., Schaepman-Strub, G., Schaepman, M. E., & Shimizu, K. K. (2017). Genomics meets remote sensing in global change studies: monitoring and predicting phenology, evolution and biodiversity. *Current Opinion in Environmental Sustainability*, 29, 177–186.
- Yan, D., Zhang, X., Yu, Y., & Guo, W. (2017). Characterizing Land Cover Impacts on the Responses of Land Surface Phenology to the Rainy Season in the Congo Basin. *Remote Sensing*, 9(5), 461.
- Yasuda, M., Matsumoto, J., Osada, N., Ichikawa, S., Kachi, N., Tani, M., Okuda, T., Furukawa, A., Nik, A. R., & Manokaran, N. (1999). The Mechanism of General Flowering in *Dipterocarpaceae* in the Malay Peninsula. *Journal of Tropical Ecology*. Cambridge University Press.
- Yeoh, S. H., Satake, A., Numata, S., Ichie, T., Lee, S. L., Basherudin, N., Muhammad, N., Kondo,

T., Otani, T., Hashim, M., & Tani, N. (2017). Unravelling proximate cues of mass flowering in the tropical forests of South-East Asia from gene expression analyses. *Molecular Ecology*, 26(19), 5074–5085.

Personal declaration:

I hereby declare that the submitted thesis is the result of my own, independent work. All external sources are explicitly acknowledged in the thesis.

Joan Sturm, 06.08.2018

A handwritten signature in black ink, consisting of a vertical line with a loop at the bottom, a horizontal line extending to the right, and a small loop at the top.